The Plant Cell, Vol. 18, 2294–2313, September 2006, www.plantcell.org © 2006 American Society of Plant Biologists

Tung Tree DGAT1 and DGAT2 Have Nonredundant Functions in Triacylglycerol Biosynthesis and Are Localized to Different Subdomains of the Endoplasmic Reticulum [W]

Jay M. Shockey,[a,1] Satinder K. Gidda,[b,1] Dorselyn C. Chapital,[a] Jui-Chang Kuan,[a] Preetinder K. Dhanoa,[b] John M. Bland,[a] Steven J. Rothstein,[b] Robert T. Mullen,[b,2] and John M. Dyer[a,2]

[a] U.S. Department of Agriculture, Agricultural Research Service, Southern Regional Research Center, New Orleans, Louisiana 70124

[b] Department of Molecular and Cellular Biology, University of Guelph, Guelph, Ontario N1G 2W1, Canada

Seeds of the tung tree (*Vernicia fordii*) produce large quantities of triacylglycerols (TAGs) containing ~80% eleostearic acid, an unusual conjugated fatty acid. We present a comparative analysis of the genetic, functional, and cellular properties of tung type 1 and type 2 diacylglycerol acyltransferases (DGAT1 and DGAT2), two unrelated enzymes that catalyze the committed step in TAG biosynthesis. We show that both enzymes are encoded by single genes and that *DGAT1* is expressed at similar levels in various organs, whereas *DGAT2* is strongly induced in developing seeds at the onset of oil biosynthesis. Expression of DGAT1 and DGAT2 in yeast produced different types and proportions of TAGs containing eleostearic acid, with DGAT2 possessing an enhanced propensity for the synthesis of trieleostearin, the main component of tung oil. Both DGAT1 and DGAT2 are located in distinct, dynamic regions of the endoplasmic reticulum (ER), and surprisingly, these regions do not overlap. Furthermore, although both DGAT1 and DGAT2 contain a similar C-terminal pentapeptide ER retrieval motif, this motif alone is not sufficient for their localization to specific regions of the ER. These data suggest that DGAT1 and DGAT2 have nonredundant functions in plants and that the production of storage oils, including those containing unusual fatty acids, occurs in distinct ER subdomains.

INTRODUCTION

Engineering temperate oilseed crops to produce novel value-added oils has been a long-standing goal of academic researchers and the biotechnology industry. Many of these oils hold great promise for use in human and animal nutritional regimes, and several others may serve as renewable chemical feedstocks that could replace petroleum-based products in industrial applications (reviewed in Jaworski and Cahoon, 2003; Dyer and Mullen, 2005; Singh et al., 2005). For instance, the seed oils of many exotic plant species contain high amounts of unusual fatty acids (e.g., epoxy, hydroxy, conjugated, or acetylenic) that can serve as raw materials for the production of inks, dyes, coatings, and a variety of other bio-based products. Large-scale production of these oils through traditional farming is often impossible because of the poor agronomic traits of these plant species. Furthermore, efforts to transfer genes encoding the proteins responsible for unusual fatty acid biosynthesis to higher yielding plants have generally met with limited success, with much lower amounts of the desired fatty acid accumulating in the oils of transgenic plants (15 to 30%) compared with the native plant species (up to 90%) (Thelen and Ohlrogge, 2002; Jaworski and Cahoon, 2003; Singh et al., 2005). It is clear from these studies that additional genes and significantly more knowledge of seed oil biosynthesis are needed before plants can be engineered to produce industrially important oils.

There are three major biosynthetic events involved in the production of seed storage oils. The first involves the synthesis of fatty acids in plastids. The second involves the modification of these fatty acids by enzymes located primarily in the endoplasmic reticulum (ER). The third involves the packaging of the nascent fatty acids into triacylglycerols (TAGs), which subsequently accumulate in oil bodies that bud off from the ER. Although a significant amount of information is currently available regarding the synthesis and modification of fatty acid structures (including the synthesis of unusual fatty acids) (Ohlrogge and Browse, 1995; Shanklin and Cahoon, 1998), much less is understood about the enzymes and cellular mechanisms required for the selection and transfer of fatty acids into storage TAGs.

Biochemical analyses have shown that TAG is synthesized in the ER by at least two pathways. The first involves the acyl-CoA–independent transfer of fatty acids from phospholipids to the *sn*-3 position of diacylglycerol to form TAG. This reaction is catalyzed by phospholipid:diacylglycerol acyltransferase (PDAT) (Dahlqvist et al., 2000; Ståhl et al., 2004). TAG is also produced via three successive acylation reactions of the hydroxyl groups of glycerol, starting from glycerol-3-phosphate, with diacylglycerol acyltransferase (DGAT)

[1] These authors contributed equally to this work.

[2] To whom correspondence should be addressed. E-mail rtmullen@uoguelph.ca or jdyer@srrc.ars.usda.gov; fax 519-837-2075 or 504-286-4367.

The authors responsible for distribution of materials integral to the findings presented in this article in accordance with the policy described in the Instructions for Authors (www.plantcell.org) are: Robert T. Mullen (rtmullen@uoguelph.ca) and John M. Dyer (jdyer@srrc.ars.usda.gov).

[W] Online version contains Web-only data.

www.plantcell.org/cgi/doi/10.1105/tpc.106.043695

catalyzing the committed step: the transfer of a fatty acyl moiety from acyl-CoA to the *sn*-3 position of diacylglycerol (Kennedy, 1961). As such, DGAT plays an essential role in controlling both the quantitative (Ichihara et al., 1988) and qualitative (Vogel and Browse, 1996; He et al., 2004a) flux of fatty acids into storage TAGs.

DGAT enzyme activity is encoded by at least two classes of genes in eukaryotic cells. The type 1 class of DGAT enzymes (DGAT1) was discovered first in mouse based on homology with mammalian acyl-CoA:cholesterol acyltransferase genes (Cases et al., 1998); subsequently, other *DGAT1* genes were identified and characterized in several plant species (Hobbs et al., 1999; Routaboul et al., 1999; Zou et al., 1999; Bouvier-Navé et al., 2000; Nykiforuk et al., 2002; He et al., 2004b; Milcamps et al., 2005). For instance, the *Arabidopsis thaliana DGAT1* gene has been shown to contribute significantly to seed TAG biosynthesis, both by overexpression (Jako et al., 2001) and through mutational down-regulation studies (Katavic et al., 1995; Routaboul et al., 1999). The type 2 class of DGAT enzymes (DGAT2) also has been identified in a number of eukaryotes, including fungi, *Caenorhabditis elegans*, human, and *Arabidopsis* (Cases et al., 2001; Lardizabal et al., 2001). The physiological function(s) of these DGAT2 enzymes in plants, however, has not been determined. Characterizing the subcellular properties of these enzymes would provide new insight into the underlying mechanisms of oil biosynthesis. This knowledge may be especially important for the production of seed oils containing unusual fatty acids, because these structures are generally incompatible with normal membrane lipids and the spatial separation of lipid biosynthetic enzymes in the ER may provide an efficient mechanism for channeling these unusual fatty acids into storage oils.

We are studying the tung tree (*Vernicia fordii*) as a model system for the production of seed storage oils that contain high amounts of industrially important fatty acids, with the end goal of transferring appropriate sets of genes to high-yielding oilseed crops for industrial oil production. Tung oil contains 80% (w/w total fatty acids) α-eleostearic acid, an unusual trienoic fatty acid (18:3$\Delta^{9cis,11trans,13trans}$) that imparts industrially useful drying qualities to the oil (Sonntag, 1979). We previously identified and characterized the enzymes and cofactor proteins required for the production of fatty acid components in tung oil, including fatty acid desaturase (FAD) and FAD-related enzymes (Dyer et al., 2002a, 2004), cytochrome b_5 (Cb5) (Hwang et al., 2004), and Cb5 reductase (Shockey et al., 2005).

Here, we provide a detailed functional and cellular analysis of tung DGAT1 and DGAT2. We show that tung DGAT1 and DGAT2 enzymes are each encoded by single genes, and that *DGAT1* is expressed at similar levels in leaves, flowers, and developing seeds, whereas *DGAT2* is strongly induced in seeds during tung oil synthesis. Furthermore, although both enzymes synthesized TAGs in a yeast functional complementation assay, DGAT2 showed a clear preference for the production of trieleostearin, the major TAG in tung oil. We also present data from subcellular localization and selective photobleaching experiments of DGAT enzymes transiently expressed in tobacco (*Nicotiana tabacum*) suspension cells indicating that they are localized to specific, dynamic regions of the ER, and furthermore, that these regions are not shared by the two enzymes. Investigation of the molecular targeting signals within DGAT1 and DGAT2 revealed that both proteins contain a similar cytosolically exposed C-terminal pentapeptide ER retrieval motif responsible for maintaining their steady state localization in the ER. Notably, this motif is not sufficient for targeting a reporter protein to the ER subdomains enriched with full-length DGAT1 or DGAT2 protein, indicating that additional portions of DGAT1 and DGAT2, including portions potentially involved in homotypic oligomerization, are required for targeting to ER subdomains. Together, these results suggest that DGAT1 and DGAT2 enzymes perform different roles in plant cells and that the production of TAGs by each enzyme occurs in specialized regions of the ER. The implications for plant lipid metabolism and the engineering of crops to produce industrially important oils are discussed.

RESULTS

DGAT1 and *DGAT2* Represent Distinct Gene Families in Higher Eukaryotes

To identify full-length coding sequences for type 1 and type 2 tung DGAT enzymes, sequences of high similarity in other *DGAT* genes were used to identify DGAT cDNAs by standard homology-based cloning techniques (details are provided in Methods). Alignment of the deduced amino acid sequences of DGAT1 or DGAT2 from tung, *Arabidopsis*, and rice (*Oryza sativa*) revealed that the proteins in each family share ~50% identity (Figures 1A and 1B), but comparisons of the two groups of proteins revealed striking differences. For instance, DGAT1 proteins are ~500 amino acids in length with 10 predicted transmembrane domains (TMDs) (Figure 1A), whereas DGAT2 proteins are ~320 amino acids long with two predicted TMDs (Figure 1B).

The evolutionary relationships within the DGAT superfamily were analyzed by performing a phylogenetic comparison with an expanded set of protein sequences from evolutionarily diverse organisms (Figure 1C). The resulting cladogram contains two main branches, made up entirely of either type 1 or type 2 DGAT sequences. Although the two human protein sequences (Hs DGAT1 and Hs DGAT2 [Oelkers et al., 1998]) do not cluster tightly with the plant sequences, it is clear that the Hs DGAT1 sequence is more similar to plant type 1 DGATs than to type 2 sequences, whereas the opposite is true for Hs DGAT2. The complete lack of similarity between type 1 and type 2 DGAT proteins indicates that the DGAT family likely represents a case of functional convergent evolution. In addition, the presence of both *DGAT1* and *DGAT2* genes in distantly related organisms (except in *Saccharomyces cerevisiae*, which contains only a type 2 DGAT enzyme called acyl-coenzyme A:diacylglycerol acyltransferase 1 [DGA1] [Oelkers et al., 2002]) suggests that both genes are ancient, having arisen before the evolutionary split between humans and plants.

Tung DGAT1 and DGAT2 Are Encoded by Single Genes, and *DGAT2* Is Highly Expressed during Tung Seed Oil Biosynthesis

To further investigate the differences in *DGAT1* and *DGAT2* gene families, the genes corresponding to the tung cDNAs were cloned. Comparison of the genomic architecture of each gene revealed

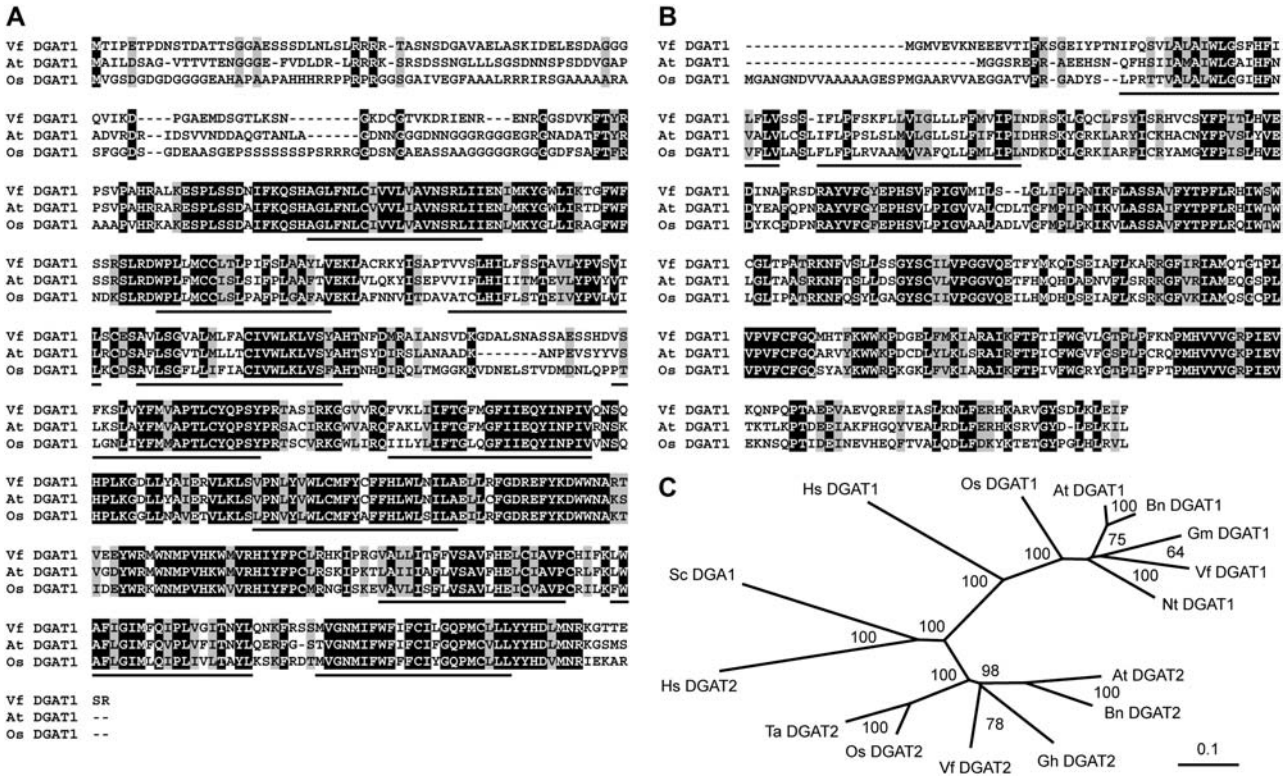

Figure 1. Sequence Alignments and Phylogenetic Comparisons of DGAT1 and DGAT2 Proteins.

(A) Multiple sequence alignment of deduced amino acid sequences of DGAT1 proteins from tung (Vf), *Arabidopsis* (At), and rice (Os). Identical residues are shaded black, and similar residues are shaded gray. Transmembrane domains, as predicted by the TMHMM server (http://www.cbs.dtu.dk/services/TMHMM-2.0/) (Krogh et al., 2001), are underlined.

(B) Alignment of DGAT2 protein sequences. Proteins are labeled as in **(A)**.

(C) Phylogenetic analysis of various cloned and annotated DGAT sequences from plants, humans, and/or *S. cerevisiae*. Each plant species is represented by either *DGAT1* or *DGAT2*, or both, depending on the availability of database sequences. The branch lengths of the tree are proportional to divergence. The 0.1 scale represents 10% change. Bootstrap values are shown in percentages at nodes. Proteins used in the analysis were DGAT1 and/or DGAT2 sequences from tung (Vf), *Arabidopsis* (At), *Brassica napus* (Bn), cotton (*Gossypium hirsutum*; Gh), rice (Os), soybean (*Glycine max*; Gm), tobacco (Nt), wheat (*Triticum aestivum*; Ta), human (Hs), and yeast (Sc).

that their intron/exon organizations were entirely different (Figure 2A), and genomic DNA gel blot analyses indicated that single copies of each gene exist in the tung genome (Figure 2B).

The potential roles of the tung *DGAT* genes were investigated by analyzing their organ-specific expression patterns, with particular emphasis on their temporal regulation during seed development. As shown in Figure 2C, both *DGAT1* and *DGAT2* transcripts accumulated at low levels in leaves and were slightly increased in flowers. During seed development, *DGAT1* transcripts were upregulated only slightly and reached a maximum at or beyond mid-August, a time point at which both eleostearic acid and total seed oil had already accumulated to ~50% of their respective maximum levels (cf. Figures 2C and 2D). Tung *DGAT2* transcripts, on the other hand, were strongly upregulated in developing seeds in mid-July, just before the onset of rapid eleostearic acid and total seed TAG accumulation (cf. Figures 2C and 2D). Collectively, these data suggest that DGAT1 plays a more constitutive role in TAG metabolism in various tung tissues, whereas DGAT2 functions more directly in the production of seed-specific TAGs containing eleostearic acid.

DGAT1 and DGAT2 Show Minor Differences in Substrate Selectivity in Vitro

To investigate the functional properties of tung DGAT1 and DGAT2 enzymes, microsomal membranes were prepared from mutant yeast cells disrupted in endogenous DGAT and PDAT enzyme activities (Δ*dga1* Δ*lro1*, strain SCY1998 [Oelkers et al., 2002]) but expressing myc epitope–tagged versions of either tung DGAT protein. Isolated microsomal membranes were then incubated with one of four different radiolabeled acyl-CoAs, palmitoyl-CoA (16:0), oleoyl-CoA (18:1), linoleoyl-CoA (18:2), or α-linolenoyl-CoA (18:3), combined with one of three different unlabeled diacylglycerol substrates, *sn*-1,2-diolein (di18:1), *sn*-1,2-dilinolein (di18:2), or *sn*-1,2-dilinolenin (di18:3). Figure 3 shows that DGAT1 enzyme activity varied widely depending on the combination of substrates used, with 18:2-CoA plus di18:2 and 18:3-CoA plus di18:1 yielding the highest levels of activity. DGAT2 had lower levels of activity overall compared with DGAT1, possibly because of the relatively lower steady state levels of DGAT2 protein detected by anti-myc protein gel blotting (data not shown).

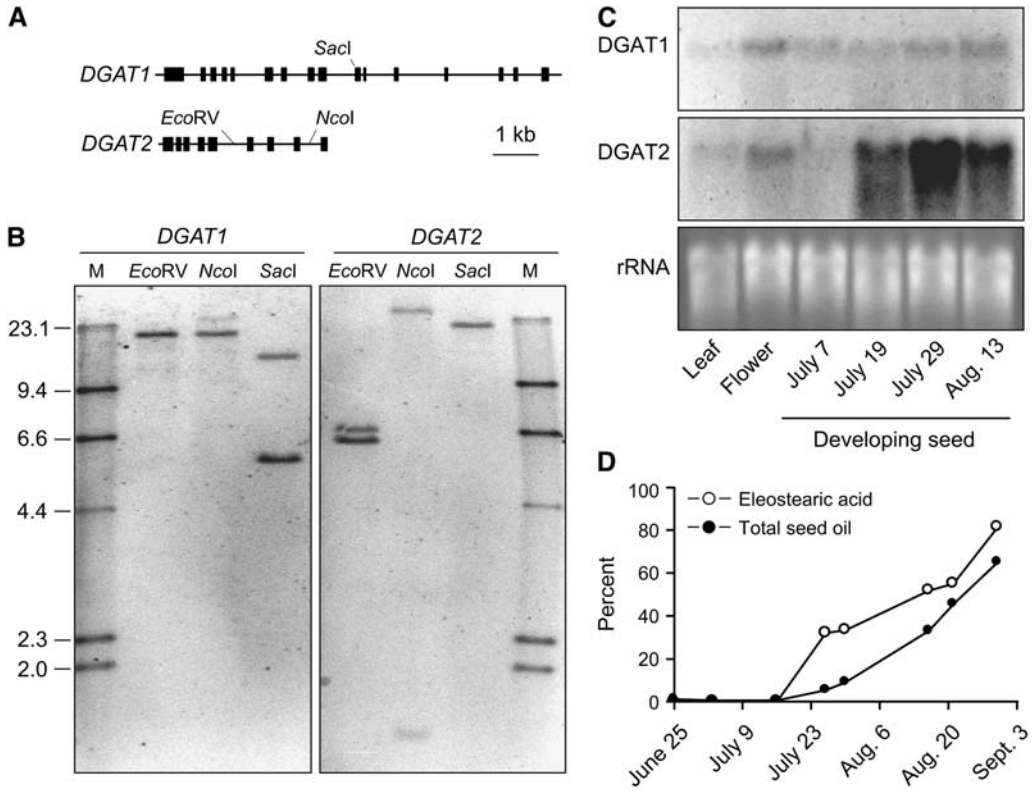

Figure 2. Genomic Organization and Expression Patterns of Tung *DGAT1* and *DGAT2* Genes in Relation to Tung Seed Oil Biosynthesis.

(A) Intron/exon structure of tung *DGAT1* and *DGAT2* genes. All exons (black boxes) and introns (lines) are drawn to scale, and the relative positions of restriction sites used for DNA gel blotting in **(B)** are shown.

(B) DNA gel blot of tung genomic DNA digested with *Eco*RV, *Nco*I, or *Sac*I and hybridized with digoxigenin (DIG)-labeled full-length ORF probes for either *DGAT1* or *DGAT2*. DIG-labeled λ *Hin*dIII molecular mass markers, in kilobase pairs, are shown at left or right (M).

(C) RNA gel blot analysis of *DGAT1* and *DGAT2* gene expression. RNA was extracted from leaves, flowers, and developing seeds, and *DGAT1* and *DGAT2* transcripts were characterized using gel blot analysis with DIG-labeled *DGAT1*- or *DGAT2*-specific probe. Ethidium bromide–stained rRNA from each sample is shown as a loading control.

(D) Accumulation of tung oil in developing tung seeds. Tung fruit were harvested throughout the growing season (June 25 to September 3), and changes in total seed oil (percentage dry weight) and eleostearic acid (percentage [w/w] total fatty acid methyl esters) contents are shown.

However, DGAT2 did show a modest preference for 18:3-CoA as the acyl donor, possessing higher activity with this acyl-CoA (regardless of the acyl acceptor diacylglycerol species) than with any of the other acyl-CoAs tested (Figure 3). Eleostearoyl-CoA and eleostearate-containing diacylglycerol substrates could not be tested with DGAT1 or DGAT2 in this in vitro assay system, because these substrates are sensitive to heat, oxidation, and acidic pH (Sonntag, 1979), making their synthesis problematic.

Tung DGAT2 Preferentially Incorporates Eleostearic Acid into TAGs in Vivo

To evaluate the ability of each tung DGAT enzyme to produce TAGs containing eleostearic acid, we used a novel functional complementation assay in which wild-type or mutant yeast cells (Δ*dga1* Δ*lro1*) were cultivated in the presence of exogenously added tung oil and a nonspecific lipase from *Candida rugosa*. Digestion of tung oil by lipase activity released eleostearic acid into the growth medium, which was subsequently taken up and incorporated into yeast lipids. Expression of tung DGAT1 and DGAT2 in Δ*dga1* Δ*lro1* cells allowed these enzymes to act upon the endogenously synthesized eleostearoyl-containing substrates to produce TAGs. Comparative analysis of TAG profiles produced by each DGAT enzyme provided insight into potential differences in their substrate selectivity.

Cultivation of wild-type yeast cells (harboring an empty pYes3 expression plasmid) in the presence of tung oil and lipase, followed by extraction of yeast lipids and analysis of fatty acid composition by gas chromatography (GC), revealed that eleostearic acid accounted for ~22% of cellular fatty acid composition (Figure 4A, WT+pYes3). Separation and analysis of TAGs by HPLC with photodiode array detection (HPLC-PDA) demonstrated that eleostearic acid was incorporated into a variety of TAG species by the endogenous yeast DGA1 or LRO1 enzyme (Figure 4B, WT+pYes3). Cultivation of mutant yeast cells harboring disruptions in the *DGA1* and *LRO1* genes, however, showed a reduction in eleostearic acid content to ~8% (Figure 4A, MUT+pYes3), and no TAGs were identified in these cells by either thin layer

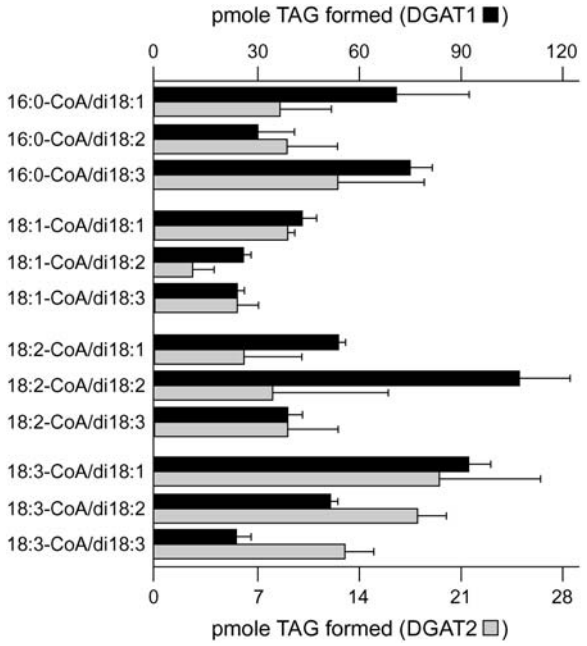

Figure 3. Biochemical Activity of DGAT Enzymes in Vitro.

Myc-tagged tung DGAT1 and DGAT2 were expressed individually in mutant yeast cells that lacked the ability to synthesize appreciable amounts of TAG, and then microsomal fractions were isolated and incubated with combinations of radiolabeled fatty acyl-CoAs and diacylglycerols. Fatty acyl-CoAs were palmitoyl-CoA (16:0-CoA), oleoyl-CoA (18:1-CoA), linoleoyl-CoA (18:2-CoA), and α-linolenoyl-CoA (18:3-CoA). Diacylglycerols were diolein (di18:1), dilinolein (di18:2), and dilinolenin (di18:3). Amounts (in picomoles per hour) of radiolabeled TAG formed per 25 μg of yeast microsomal membrane protein minus the amount of TAG produced in control experiments lacking exogenous DAG substrates are shown for each condition (average ± SD of three independent experiments). See Methods for additional details.

chromatography (TLC) (Figure 4A, MUT+pYes3) or HPLC-PDA (Figure 4B, MUT+pYes3). Transformation of mutant yeast cells with a plasmid-borne copy of the *DGA1* gene restored TAG biosynthesis (Figures 4A and 4B, MUT+DGA1), thereby establishing a functional complementation assay for DGAT enzyme activity.

Transformation of mutant yeast cells with a plasmid-borne copy of tung DGAT1 also restored TAG biosynthesis (Figure 4A, MUT+DGAT1), and the pool of TAGs produced by DGAT1 was similar to that of yeast DGA1, with the exception of reduced amounts of linoleoyl-dieleostearoyl-glycerol and dilinoleoyl-eleostearoyl-glycerol in samples derived from tung DGAT1 (Figure 4B, cf. MUT+DGA1 and MUT+DGAT1). Expression of tung DGAT2 in the mutant yeast cells, however, resulted in a significant increase in trieleostearin content and a decrease in monoeleostearoyl-containing TAGs compared with TAGs produced by either yeast DGA1 or tung DGAT1 (Figure 4B, MUT+DGAT2). Trieleostearin accounted for 11.1 ± 2.1% ($n = 3$) of all eleostearoyl-containing TAGs in samples derived from DGAT2 (calculated by dividing the integrated peak area of trieleostearin by the sum of all peak areas in the chromatogram) but only 2.7 ± 0.2% and 2.1 ± 0.1% of TAGs produced by yeast DGA1 and tung DGAT1, respectively. These data demonstrate that tung DGAT2 possesses an approximately fivefold preference for the synthesis of trieleostearin compared with the amount synthesized by tung DGAT1. Tung DGAT2 also showed preferential synthesis of TAGs containing polyunsaturated fatty acids, as indicated by the accumulation of linoleoyl-dieleostearoyl-glycerol and dilinoleoyl-eleostearoyl-glycerol in favor of the monounsaturate-containing TAGs dieleostearoyl-palmitoleoyl-glycerol and eleostearoyl-dipalmitoleoyl-glycerol, which were favored by tung DGAT1 (Figure 4B).

Together, the data presented in Figure 4 indicate that tung DGAT1 and DGAT2 produce different pools of TAGs under in vivo, steady state conditions and that DGAT2 shows an increased propensity for the formation of trieleostearin, the main component of tung oil.

DGAT1 and DGAT2 Proteins Are Enriched in Subdomains of the ER

Previous in vitro experiments demonstrated that DGAT enzyme activity was associated with microsomal membrane preparations (Figure 3) (Cao and Huang, 1986; Settlage et al., 1995; Lacey and Hills, 1996). To perform a more detailed investigation of the subcellular properties of these enzymes in plant cells, we expressed myc epitope–tagged tung DGAT1 or DGAT2 in tobacco BY-2 suspension cells and then examined their immunofluorescence staining patterns by confocal laser-scanning microscopy (CLSM). The addition of the myc tag provided a means to distinguish between tung DGAT1 and DGAT2 and endogenous tobacco DGAT proteins (Bouvier-Navé et al., 2000) but likely did not interfere with their folding or function, because both myc-tagged DGAT1 and DGAT2 possessed enzyme activities similar to their native protein counterparts when expressed in yeast (see Supplemental Figure 3 online).

As shown in Figure 5, both myc-DGAT1 and myc-DGAT2 displayed reticular immunofluorescence patterns similar to the staining pattern of endogenous ER labeled with fluor-conjugated concanavalin A (ConA). Interestingly, close inspection of these cells at higher magnification revealed that myc-DGAT1 and myc-DGAT2 were not distributed uniformly throughout the ConA-stained ER but rather were enriched in distinct regions of the ER (Figure 5, white arrowheads). Other portions of the ER, however, contained relatively low amounts of myc-tagged DGAT1 or DGAT2 protein fluorescence compared with the ConA fluorescence in these same regions (Figure 5, black arrowheads). Similar results were observed when the ER in myc-DGAT1 or myc-DGAT2 cells was labeled with 3,3′-dihexyloxacarbocyanine iodide, another commonly used stain for the general ER (Sabnis et al., 1997) (see Supplemental Figure 4 online).

Fluorescence recovery after photobleaching (FRAP) experiments were performed with DGAT2 tagged at its N terminus with a monomeric form of the green fluorescent protein (GFP-DGAT2) to investigate the mobility of proteins in these subdomains. Similar to the myc epitope–tagged variant of DGAT2, the enzyme activity of the GFP-DGAT2 fusion protein was nearly identical to that of native DGAT2 (see Supplemental Figure 3 online). As shown in Figure 6, the fluorescence attributable to GFP-DGAT2 recovered rapidly (half-time = 23.9 ± 7.2 s [$n = 11$]) after photobleaching of a selective region of the ER where the fusion

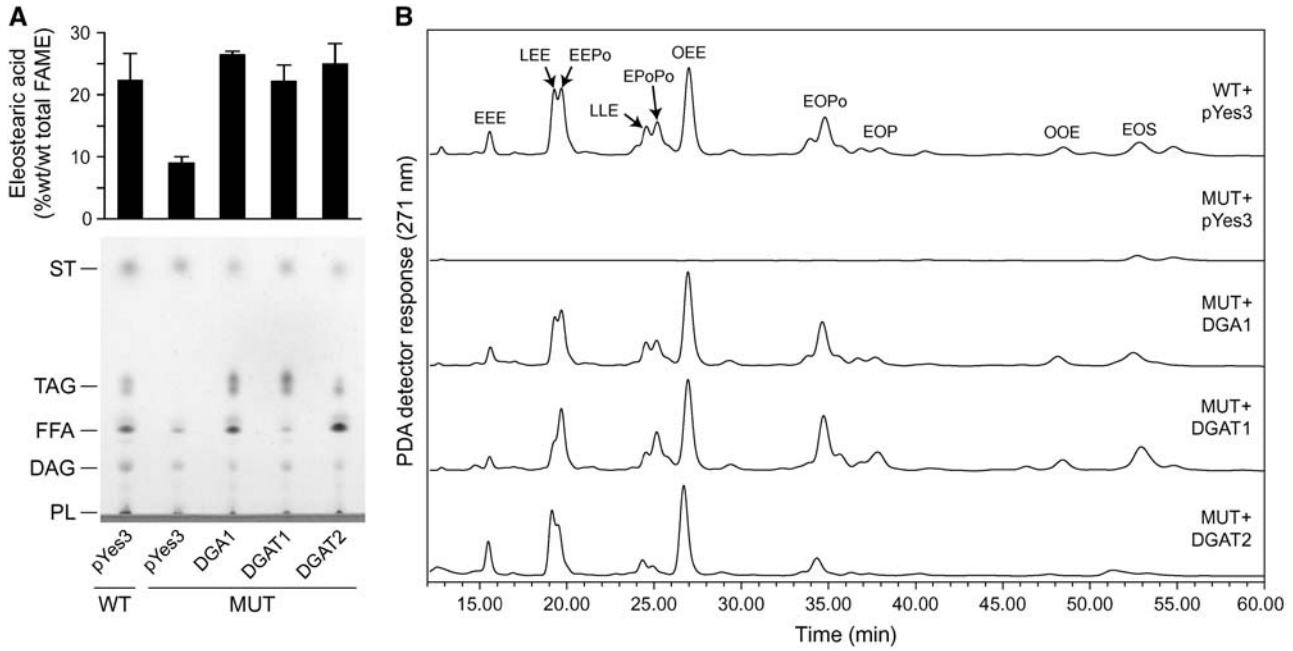

Figure 4. Functional Analysis of DGAT Enzymes in Vivo.

Wild-type (WT) and mutant (MUT; lacking the ability to produce TAGs) yeast cells were cultivated in the presence of tung oil and a nonspecific lipase, cells were harvested, and lipids were extracted for the identification of eleostearoyl-containing compounds. Yeast cells were also transformed with an empty plasmid (pYes3) or a plasmid expressing yeast *DGA1*, tung *DGAT1*, or tung *DGAT2*. Strain and plasmid combinations are shown along the bottom of **(A)** and at right in **(B)**.

(A) The top panel shows the percentage of eleostearic acid in yeast cells complemented with various DGAT1 or DGAT2 enzymes, as determined by GC-FID analysis (average ± SD, $n = 3$). The bottom panel shows a TLC separation of various lipid classes. Positions of lipid standards are shown at left: diacylglycerol (DAG), free fatty acids (FFA), phospholipids (PL), sterol esters (ST), and triacylglycerols (TAG). Samples are representative of three independent experiments. Note the reduction of eleostearic acid (top panel) and the absence of TAGs (bottom panel) in the MUT+pYes3 yeast strain.

(B) HPLC-PDA analysis of yeast lipids. Lipids were extracted from yeast cells and then separated and analyzed by HPLC with PDA detection. The PDA device monitored UV light absorbance from 210 to 345 nm, which allowed the detection of eleostearoyl-containing compounds by virtue of the characteristic UV light absorbance spectrum of eleostearic acid (see Supplemental Figure 1 online for a complete PDA data set of WT+pYes3 lipids and a comparison with a tung oil standard). Each chromatogram shown represents the 271-nm absorbance trace (λ_{max} of eleostearic acid) extracted from the complete PDA data set. TAGs were identified by comparison of peak retention times and retention times of authentic standards, and assignments were confirmed by liquid chromatography-mass spectrometry (LC-MS) (see Supplemental Figure 2 online). Each TAG peak is labeled according to the three fatty acyl side chains, although stereospecific positions are not known. Fatty acid abbreviations are as follows: eleostearic (E), linoleic (L), oleic (O), palmitic (P), palmitoleic (Po), and stearic (S). Each chromatogram is representative of three independent experiments.

protein was enriched, indicating that at least a portion of the GFP-DGAT2 proteins move to and from these regions of the ER. No significant recovery of GFP-DGAT2 fluorescence was observed, however, when cells were killed by formaldehyde fixation before photobleaching (Figure 6B). Likewise, unbleached areas of the ER in GFP-DGAT2–transformed cells displayed no significant loss of fluorescence intensity (data not shown).

DGAT1 and DGAT2 Occupy Different Subdomains of the ER

To determine whether the distinct regions of the ER occupied by tung DGAT1 and DGAT2 are shared between these two proteins, tobacco cells were cotransformed with myc-DGAT1 and GFP-DGAT2. As shown in Figure 7 (top panels), high-magnification CLSM revealed that the immunofluoresence patterns attributable to myc-DGAT1 and GFP-DGAT2 did not colocalize but rather were juxtaposed at different regions of the ConA-stained ER. Similar lack of colocalization was observed when myc-DGAT1 was coexpressed with a hemagglutinin epitope–tagged version of DGAT2 (HA-DGAT2) (see Supplemental Figure 5 online) or when HA-DGAT1 was coexpressed with myc-DGAT2 (or GFP-DGAT2) (data not shown). Together, these results indicate that the regions of the ER network occupied by DGAT1 or DGAT2 are not shared but rather represent different subdomains.

As additional control experiments, coexpression of both HA- and myc-tagged DGAT2 revealed that these differentially tagged DGAT2 proteins colocalized exclusively in the same regions of the ER (Figure 7, middle panels), indicating that the accumulation of DGAT1 and DGAT2 in unique ER subdomains was not attributable to their appendage to different epitope tags (or to GFP for DGAT2). In addition, coexpression of HA-DGAT2 and a myc-tagged Cb5 (myc-Cb5) resulted in only partial colocalization (Figure 7, bottom panels), similar to the results obtained when the ER in DGAT1- or DGAT2-transformed cells was stained with ConA or 3,3′-dihexyloxacarbocyanine iodide

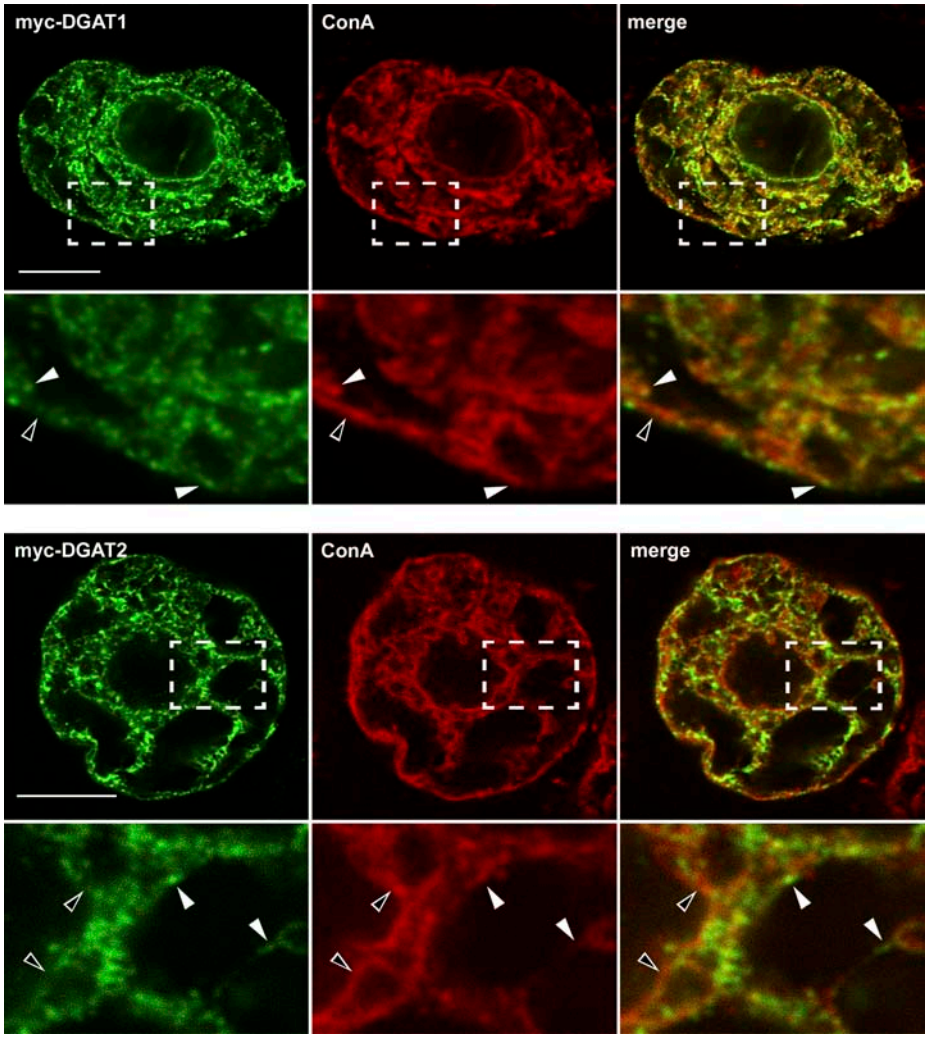

Figure 5. Subcellular Localization of DGAT1 and DGAT2 in Tobacco BY-2 Cells.

BY-2 cells were transformed transiently with either myc-DGAT1 or myc-DGAT2, fixed in formaldehyde at 4 h after biolistic bombardment, and then processed for immunofluorescence CLSM. Hatched boxes represent the portion of the cell shown at higher magnification in the panels below. The yellow/orange color in the merged images indicates the colocalization of expressed myc-DGAT1 or myc-DGAT2 and endogenous ER stained with ConA conjugated to Alexa 594 in the same cells; white arrowheads also indicate colocalizations. Black arrowheads indicate regions of ConA-stained ER that contain relatively low immunofluorescence attributable to myc-DGAT1 or myc-DGAT2. Bars = 10 μm.

(Figure 5; see Supplemental Figure 4 online). These latter data reinforce the premise that the localization of DGATs to specific ER subdomains was not an artifact of their appended epitope tags (because Cb5 was tagged with the myc epitope sequence) or of their transient (over)expression (because expressed myc-Cb5 localized throughout the entire ER network in transformed tobacco cells, as reported elsewhere) (Hwang et al., 2004) (cf. the colocalization of the reticular immunofluoresence patterns attributable to myc-Cb5 and ConA-stained ER in Figure 7, bottom panels). Indeed, the ER subdomains occupied by DGAT1 and DGAT2 also were shown to be different from at least one other previously characterized ER subdomain involved in calcium partitioning (Papp et al., 2003), because neither myc-DGAT1 nor myc-DGAT2 colocalized with the endogenous BY-2 calcium binding protein calnexin (see Supplemental Figure 6 online). The localization of DGAT1 and DGAT2 to distinct subdomains of the ER (Figures 5 and 7) was not specific to expression in BY-2 cells, because similar results were observed when tung DGAT1 and DGAT2 were transiently expressed in *Arabidopsis* suspension cells (data not shown). Mock-transformed tobacco and *Arabidopsis* cells yielded no immunofluorescence signal (data not shown).

The N and C Termini of DGAT1 and DGAT2 Are Oriented toward the Cytosolic Side of ER Membranes

To determine the topological orientation of DGAT1 and DGAT2 proteins in ER membranes, tobacco cells expressing N- and C-terminal myc-tagged DGAT1 (myc-DGAT1 and DGAT1-myc, respectively) or DGAT2 (myc-DGAT2 and DGAT2-myc, respectively)

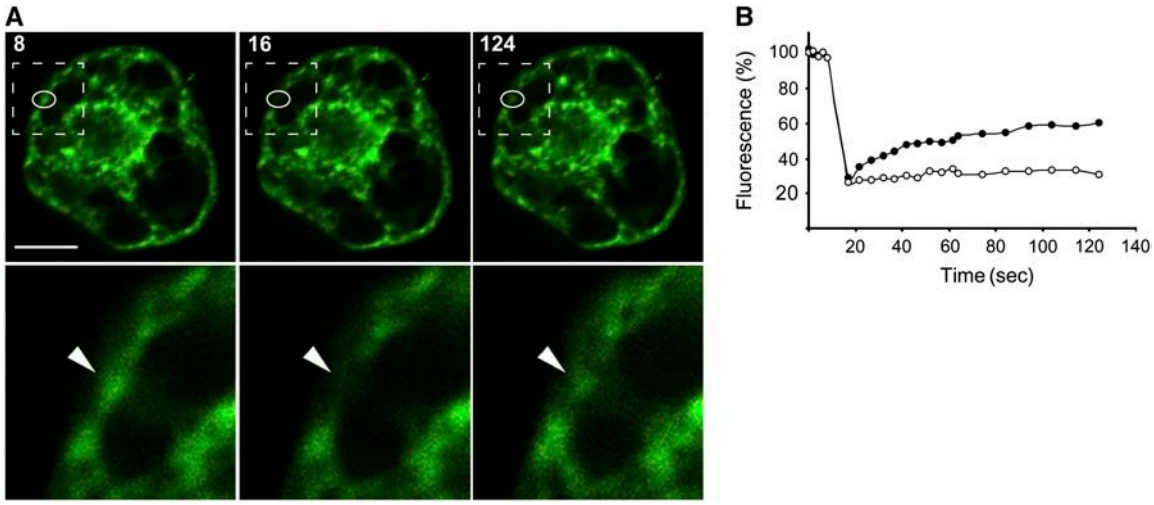

Figure 6. FRAP Analysis of GFP-DGAT2 in BY-2 Cells.

(A) Selective photobleaching of GFP-DGAT2 fluorescence in a representative transiently transformed living BY-2 cell at 4 h after biolistic bombardment. The outlined area (ovals) represents a discrete region of the ER containing GFP-DGAT2 that was photobleached and then monitored over time for the recovery of fluorescence. The time lapse is indicated in seconds at top left of each frame in the top row of images, with the last prebleached image collected represented as 8 s. The 16-s time point represents the first image collected after the photobleaching event. The other image of the postbleach recovery series (124 s) illustrates the recovery of GFP-DGAT2 fluorescence in the ER subdomain. The portion of the GFP-DGAT2–transformed cell at each time point outlined by the hatched boxes in the top row of images is shown at higher magnification in the bottom row of images; arrowheads denote the specific region of the ER containing GFP-DGAT2 that was photobleached. Note that the CLSM settings (laser power and detection gain) for imaging GFP-DGAT2 fluorescence in the BY-2 cell shown here were higher than those used for most other cells examined during FRAP experiments; lower CLSM settings in these other experiments were necessary to reduce fluorescence oversaturation. Bar = 10 μm.

(B) Fluorescence intensity recovery plots of GFP-DGAT2 in an ER subdomain in either the BY-2 cell shown in **(A)** (closed circles) or another representative GFP-DGAT2–transformed BY-2 cell that was fixed in formaldehyde at 4 h after biolistic bombardment and then subjected to photobleaching (open circles). Both fluorescence recovery curves are expressed as fluorescence percentage over the entire time series and represent the relative fluorescence intensity of a measured GFP-DGAT2–containing ER structure that was normalized to the nonbleached fluorescence in another area of the cell. One hundred percent fluorescence indicates the normalized prebleach fluorescence intensity.

proteins were fixed and then differentially permeabilized with either Triton X-100 or digitonin before immunofluorescence microscopy. Triton X-100 permeabilizes all cellular membranes in tobacco cells (Lee et al., 1997), allowing the detection of epitopes located within the cytosol (e.g., endogenous tubulin) (Figure 8Aa) and within subcellular compartments (e.g., endogenous calreticulin in the ER lumen) (Figure 8Ab) of the same cells. By contrast, digitonin permeabilizes only the plasma membrane (Lee et al., 1997), permitting the detection of cytosolic tubulin (Figure 8Ac) but not ER lumenal calreticulin (Figure 8Ad). Incubation of DGAT-transformed tobacco cells with digitonin resulted in the immunodetection of myc-DGAT1 (Figure 8Ae), myc-DGAT2 (Figure 8Ag), DGAT1-myc (Figure 8Ai), and DGAT2-myc (Figure 8Ak) but not endogenous calreticulin in the corresponding same cells (Figures 8Af, 8Ah, 8Aj, and 8Al). Thus, both the N and C termini of DGAT1 and DGAT2 are located on the cytosolic side of ER membranes, consistent with a predicted even (but different) number of TMDs for these two proteins (Figure 8B; see also Figures 1A and 1B).

DGAT1 and DGAT2 Contain Similar C-Terminal ER Retrieval Motifs

To characterize the molecular targeting signals responsible for the steady state localization of DGAT proteins in the ER, we performed an alignment of multiple DGAT1 and DGAT2 proteins to identify potential ER retrieval motifs. As shown in Figure 9A, both groups of proteins lack a C-terminal dilysine motif (-KXKXX-COOH or -KKXX-COOH) responsible for maintaining the localization of most other resident ER membrane proteins (Benghezal et al., 2000), but they do contain a motif that is similar to a recently identified pentapeptide ER retrieval motif (-ϕ-X-X-K/R/D/E-ϕ-COOH, where ϕ is any large hydrophobic amino acid residue) (McCartney et al., 2004). Notably, the putative ER retrieval motifs in DGAT1 and DGAT2 were located upstream from their C termini (Figure 9A), unlike the originally identified motif, which was positioned at the extreme C terminus (McCartney et al., 2004).

To test the role of these C-terminal residues in the ER localization of DGAT1 and DGAT2, we made use of the well-characterized type I (N_{lumen}-$C_{cytosol}$) reporter membrane protein, GFP-Cf9, which when expressed in onion (*Allium cepa*) epidermal cells serves as a model system for studying protein sorting within the secretory pathway in vivo (Scott et al., 1999; Benghazal et al., 2000; McCartney et al., 2004). As shown schematically in Figure 9B, GFP-Cf9 consists of GFP fused to the N-terminal *Arabidopsis* chitinase signal peptide and the C-terminal 74 amino acid residues of the tomato (*Solanum lycopersicum*) *Cladosporium fulvum-9* (Cf9) disease resistance gene product. This region includes the protein's single TMD and cytosol-exposed dilysine ER retrieval motif at positions –3 and –4 (underlined:

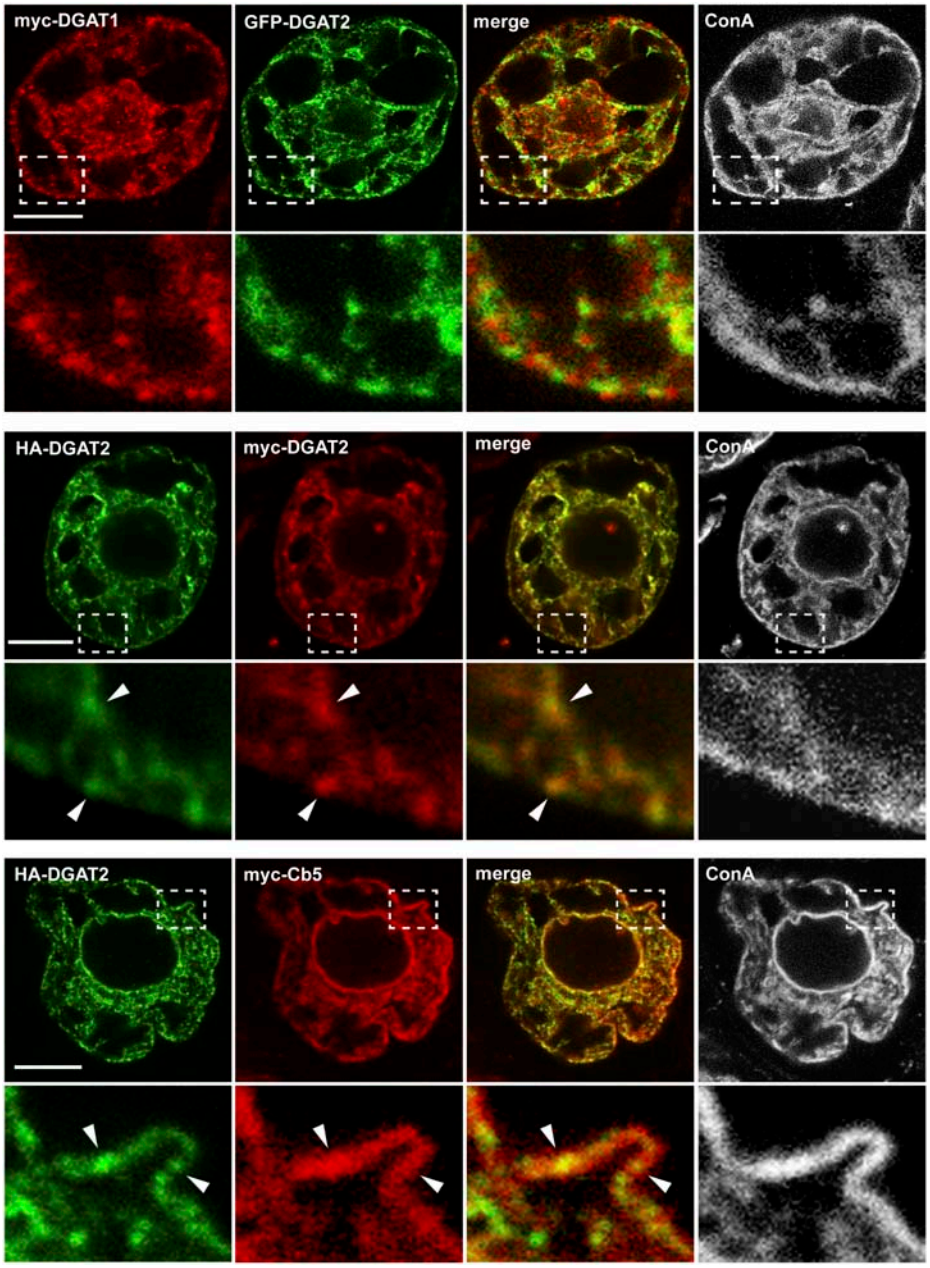

Figure 7. Subcellular Localization of Coexpressed DGAT1 and DGAT2 in BY-2 Cells.

BY-2 cells were cotransformed with either epitope- or GFP-tagged versions of tung DGAT1, DGAT2, or Cb5, fixed in formaldehyde at 4 h after biolistic bombardment, and then processed for immunofluorescence CLSM. Hatched boxes represent the portion of the cell shown at higher magnification in the panels below. Note that the fluorescence patterns attributable to coexpressed myc-DGAT1 and GFP-DGAT2 in the same cell are distinctly different; compare the nonoverlapping red and green fluorescence, respectively, in the merged images. Obvious colocalizations between coexpressed HA-DGAT2 and myc-DGAT2 in the same cell are indicated with white arrowheads. Arrowheads also highlight regions of the ER where HA-DGAT2 and myc-Cb5 colocalize in the same cotransformed cell. Endogenous ER in all cotransformed cells was stained with ConA conjugated to Alexa 594; fluorescence attributable to ConA staining is pseudocolored white. Bars = 10 μm.

-KKRY-COOH). As expected, expression of GFP-Cf9 in onion cells resulted in the steady state localization of the protein in the ER (cf. fluorescence attributable to GFP-Cf9 and coexpressed red fluorescent protein [RFP]–HDEL, a well-known ER marker protein [Haseloff et al., 1997]) (Figures 9B and 9C), whereas replacement of the C-terminal Lys residues in GFP-Cf9 with Asn (GFP-Cf9KKΔNN) disrupted the ER targeting signal, resulting in the steady state localization of the reporter protein in the plasma membrane (cf. fluorescence attributable to GFP-Cf9KKΔNN and coexpressed RFP-RhoGTPase, a well-known plasma

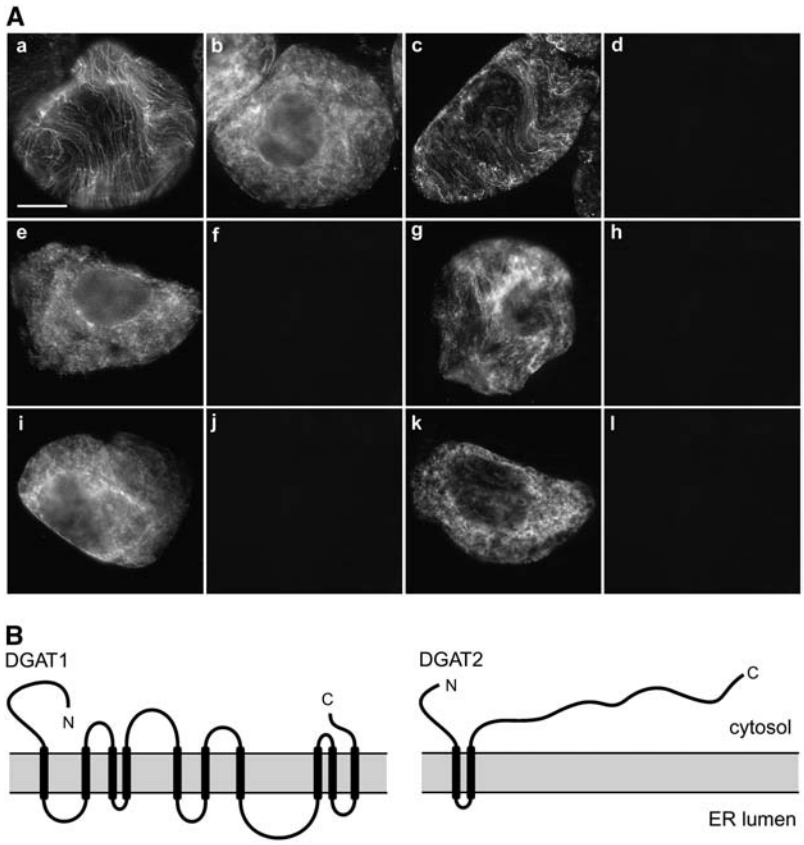

Figure 8. Topological Orientation of DGAT1 and DGAT2 in ER Membranes.

(A) Nontransformed (**[a]** to **[d]**) and transiently transformed (**[e]** to **[l]**) BY-2 cells were fixed in formaldehyde and permeabilized using either Triton X-100 (**[a]** and **[b]**), which perforates all cellular membranes, or digitonin (**[c]** to **[l]**), which selectively permeabilizes the plasma membrane, then cells were processed for immunofluorescence microscopy. Bar in **(a)** = 10 μm.

(a) and **(b)** Immunostaining attributable to endogenous tubulin in cytosolic microtubules **(a)** and calreticulin in the ER lumen **(b)** in the same nontransformed, Triton X-100–permeabilized cells.

(c) and **(d)** Presence of cytosolic tubulin **(c)** but lack of immunostaining attributable to endogenous calreticulin **(d)** in the same digitonin-permeabilized cells.

(e) to **(l)** Immunostaining attributable to transiently expressed myc-DGAT1 **(e)**, myc-DGAT2 **(g)**, DGAT1-myc **(i)**, or DGAT2-myc **(k)** but absence of fluorescence attributable to endogenous calreticulin in the corresponding (**[f]**, **[h]**, **[j]**, and **[l]**) same digitonin-permeabilized cells.

(B) Predicted topological maps of DGAT1 and DGAT2. Regions in DGAT1 and DGAT2 proposed to be hydrophobic membrane-spanning domains or hydrophilic domains facing the cytosol or ER lumen were identified using the TMHMM program (version 2.0). Based on the results presented in **(A)**, the N and C termini of DGAT1 and DGAT2 are predicted to face the cytosol.

membrane marker protein [Bischoff et al., 1990]) (Figures 9B and 9C) (McCartney et al., 2004).

Replacement of the -KKRY motif of GFP-Cf9 with the C-terminal 15 amino acid residues of tung DGAT1 resulted in localization of the protein in the ER (Figures 9B and 9C), demonstrating that this sequence could function as an ER retrieval signal (cf. fluorescence attributable to GFP-Cf9-DGAT1 with GFP-Cf9 and RFP-HDEL). Replacement of DGAT1 residues –1 to –5 or –6 to –10 with Ala had no effect on ER localization (GFP-Cf9-DGAT1ΔA1 and GFP-Cf9-DGAT1ΔA2), whereas replacement of the -YYHDL- sequence disrupted ER targeting (cf. fluorescence attributable to GFP-Cf9-DGAT1ΔA3 with GFP-Cf9KKΔNN and RFP-RhoGTPase) (Figures 9B and 9C). These data clearly demonstrate that the upstream -YYHDL- pentapeptide motif functions as an ER localization signal. Furthermore, the construct GFP-Cf9-YYHDL also was localized to the ER (Figures 9B and 9C), demonstrating that the DGAT1 pentapeptide sequence could also function at the extreme C terminus, similar to previously reported ER resident membrane proteins (McCartney et al., 2004).

Replacement of the -KKRY motif of GFP-Cf9 with the C-terminal 9 or 13 amino acid residues of tung DGAT2 (which included the -LKLEI- pentapeptide motif), however, resulted in localization of the reporter protein to both the ER and small punctate structures (GFP-Cf9-DGAT2 and GFP-Cf9-DGAT2+13 [Figure 9C, white arrowheads]), suggesting that the reporter

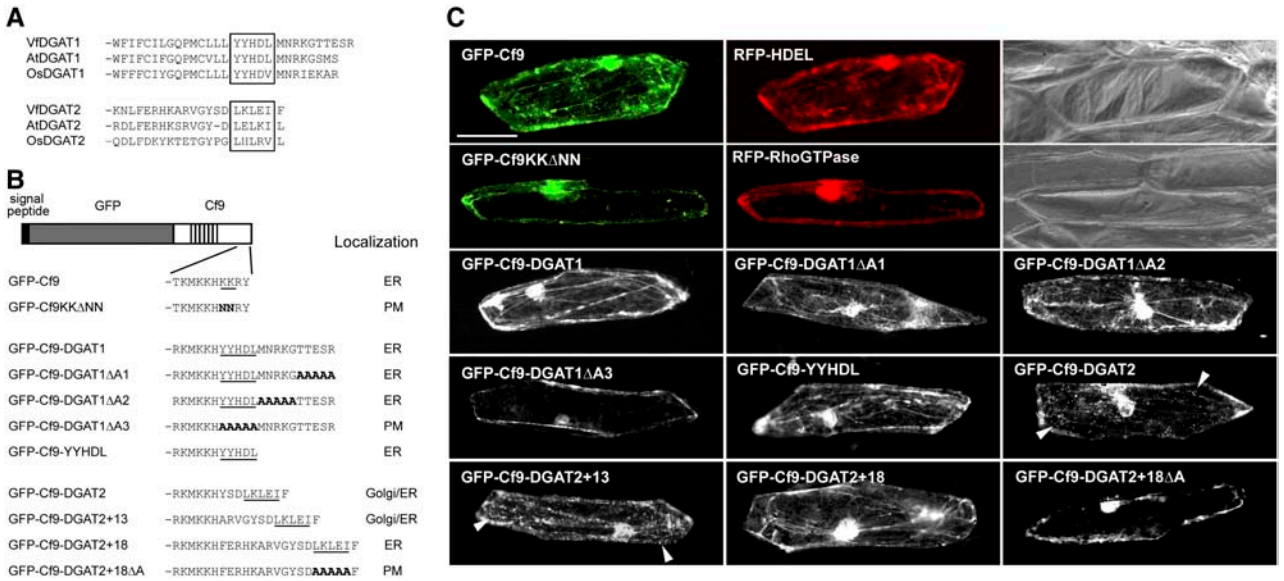

Figure 9. Localization of Various GFP-Cf9 Fusion Proteins in Onion Epidermal Cells.

(A) Deduced C-terminal amino acid sequence alignment of various DGAT1 and DGAT2 proteins from tung (Vf), *Arabidopsis* (At), and rice (Os). The putative aromatic amino acid–enriched ER retrieval motif in both groups of proteins is boxed.

(B) Schematic of the GFP-Cf9 chimeric proteins and their corresponding intracellular localization in transformed onion epidermal cells as ER, Golgi, or plasma membrane (PM). The GFP-Cf9 chimeric protein is drawn to scale and consists of an N-terminal *Arabidopsis* chitinase signal peptide (black box), the GFP (gray box), and C-terminal amino acid sequences from Cf9 (white box), including the protein's single TMD (lined box) and dilysine ER retrieval motif (underlined). The C-terminal Cf9 sequences were modified by replacing the protein's dilysine motif with either the tung DGAT1 or DGAT2 C-terminal sequence, including each protein's putative pentapeptide ER retrieval motif (underlined). Modified amino acid residues in the various GFP-Cf9 or GFP-Cf9-DGAT chimeric proteins are shown in boldface.

(C) Localization of various GFP-Cf9 and RFP fusion proteins in onion epidermal cells. Onion epidermal peels were either bombarded with DNA encoding different GFP-Cf9 chimeric proteins, as illustrated in **(B)**, or cobombarded with DNA encoding a GFP-Cf9 chimeric protein and either RFP-HDEL or RFP-RhoGTPase. Cells were then incubated for 8 h in the dark and visualized using either fluorescence or bright-field microscopy. Each representative micrograph is labeled at top left with either the name of the transiently expressed GFP-Cf9 fusion protein or the name of the coexpressed RFP fusion protein. Also shown are the corresponding bright-field micrographs of cells cotransformed with either GFP-Cf9 and RFP-HDEL or GFP-Cf9KKΔNN and RFP-RhoGTPase (two panels at top right). Arrowheads indicate individual Golgi complexes in cells transformed with GFP-Cf9-DGAT2 or GFP-Cf9-DGAT2+13. Bar = 100 μm.

protein was inefficiently retrieved from post-ER compartments. Based on their morphology, distribution, and dynamic movements, these punctate structures were assumed to be Golgi bodies, a premise that was substantiated by the colocalization of GFP-Cf9-DGAT2 and GFP-Cf9-DGAT2+13 with the coexpressed Golgi marker protein RFP-BS14a (see Supplemental Figure 7 online). GFP-Cf9 was localized entirely to the ER, however, when the fusion protein contained the C-terminal 18 amino acid residues of DGAT2 (GFP-Cf9-DGAT2+18), indicating that the context conveyed by residues upstream of the putative ER retrieval motif was essential for its proper function. As expected, replacement of the residues within the -LKLEI- sequence with Ala resulted in the protein (GFP-Cf9-DGAT2+18ΔA) being mislocalized to the plasma membrane rather than to the ER. Together, the results presented in Figure 9 demonstrate that although DGAT1 and DGAT2 each contains a C-terminal pentapeptide ER retrieval motif, the functioning of the DGAT2 motif may be more sensitive to proper protein context for correct presentation and interaction with the protein-sorting machinery.

The DGAT1 and DGAT2 C-Terminal ER Retrieval Motifs Are Not Sufficient for the Localization of Proteins to Subdomains of the ER

To determine whether the DGAT1 and/or DGAT2 C-terminal ER retrieval motifs also were involved in the localization of the DGAT proteins to subdomains of the ER, we coexpressed each GFP-Cf9 sufficiency construct (i.e., GFP-Cf9-DGAT1 or GFP-Cf9-DGAT2+18 [Figure 9B]) with its full-length protein counterpart (i.e., myc-DGAT1 or myc-DGAT2). As shown in Figure 10, both full-length DGAT proteins were localized to distinct portions of the ER, as expected (cf. with Figure 5), whereas the coexpressed GFP-Cf9 sufficiency constructs were localized throughout the entire ER network, as indicated by their complete colocalization with the fluorescence attributable to ConA-stained ER in the same cells (Figure 10). Collectively, these data indicate that although the C-terminal ER retrieval motifs of DGAT proteins function as general ER localization signals, additional portions of the DGAT protein sequence are required for targeting to specific subdomains of the ER.

DISCUSSION

Genetic and Biochemical Properties of DGAT1 and DGAT2

The biochemical activities associated with the production of TAGs in plants are well studied, but only recently have the genes associated with these enzyme activities been identified. For instance, the enzymes that catalyze the first two acylation reactions of glycerol, glycerol-3-phosphate acyltransferase (GPAT) and lysophosphatidic acid acyltransferase (LPAT), are encoded by large gene families in *Arabidopsis* (Zheng et al., 2003; Kim et al., 2005) and in other oilseed species, including tung (our unpublished data). Therefore, many possibilities exist regarding which GPAT and LPAT isoforms participate specifically in seed TAG biosynthesis. The complexity of plant *PDAT* gene families is not well characterized, although initial data suggest that at least two genes exist in *Arabidopsis* (Ståhl et al., 2004), tung (our unpublished data), and castor bean (*Ricinus communis*) (J.M. Shockey and J. Browse, unpublished data).

Conversely, initial reports describing the cloning of type 1 *DGAT* genes indicated that they constituted small, if not single-copy, gene families in plants (Bouvier-Navé et al., 2000; Nykiforuk et al., 2002; He et al., 2004a). These findings suggested that the determination of the biochemical characteristics and physiological roles of DGAT1 would be relatively easier than that of other acyltransferases and that significant control of TAG fatty acid content would be possible through the overexpression of single *DGAT1* transgenes in new host species. However, the discovery of a second type of DGAT enzyme (Lardizabal et al., 2001) complicated this scenario. Indeed, because DGAT2 enzymes are widely conserved in nature (Figure 1), they are also likely to perform one or more important metabolic functions.

Tung represents an excellent model for characterizing the functional properties of DGAT enzymes, because there are single

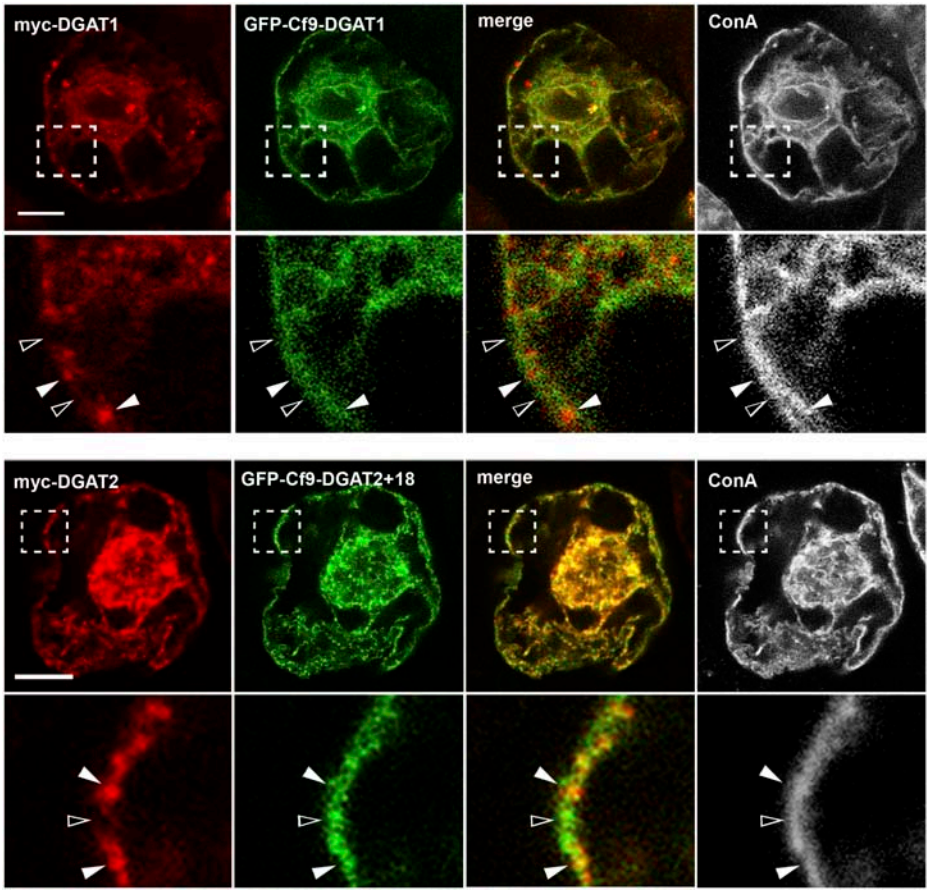

Figure 10. Localization of Coexpressed DGAT1 or DGAT2 and GFP-Cf9 Fusion Proteins in BY-2 Cells.

BY-2 cells were cotransformed with either myc-DGAT1 or myc-DGAT2 and GFP-Cf9-DGAT1 or GFP-Cf9-DGAT2+18 (see Figure 9B), fixed in formaldehyde at 4 h after biolistic bombardment, and then processed for immunofluorescence CLSM. Hatched boxes represent the portion of the cell shown at higher magnification in the panels below. Black arrowheads indicate regions of ConA-stained ER that contain GFP-Cf9-DGAT1 or GFP-Cf9-DGAT2+18 but relatively low immunofluorescence attributable to myc-DGAT1 or myc-DGAT2, respectively; compare the colocalization of GFP-Cf9-DGAT1 or GFP-Cf9-DGAT2+18 and ConA-stained ER in the same cells. The yellow/orange color in the merged images indicates colocalizations of coexpressed myc-DGAT1 or myc-DGAT2 and GFP-Cf9-DGAT1 or GFP-Cf9-DGAT2+18, respectively, in the same cells; white arrowheads indicate colocalizations. Fluorescence attributable to ConA conjugated to Alexa 594 is pseudocolored white. Bars = 10 μm.

copies of *DGAT1* and *DGAT2* in the tung genome (Figure 2) and tung seeds produce TAGs containing high amounts of the unusual fatty acid α-eleostearic acid (Sonntag, 1979). Expression of DGATs in yeast cells followed by in vitro analysis of enzyme activity in purified microsomal membranes revealed that DGAT1 and DGAT2 showed only minor differences in substrate selectivity (Figure 3), although eleostearoyl-containing substrates were not tested in this assay system. An in vivo functional assay in yeast cells, however, demonstrated that these enzymes show clear differences in their affinity for substrates containing eleostearic acid. That is, tung DGAT1 synthesized a pool of TAGs containing eleostearic acid similar to the pool produced by yeast DGA1 (Figure 4B), an enzyme that does not normally encounter eleostearic acid during TAG formation. Tung DGAT2, however, showed a clear preference for the synthesis of trieleostearin compared with yeast DGA1 and tung DGAT1. These data, coupled with the upregulation of tung DGAT2 during the synthesis of tung seed oil (Figure 2), suggest that tung DGAT1 and DGAT2 have nonredundant functions in plant cells and that DGAT2 plays a more important role in the production of trieleostearin in developing tung seeds.

Localization of DGAT1 and DGAT2 in Distinct Subdomains of the ER and Potential Role(s) of DGATs in TAG Metabolism

Inspection of the subcellular localization of tung DGAT1 and DGAT2 in tobacco BY-2 cells revealed that these proteins are enriched in distinct subdomains of the ER (Figure 5). In addition, FRAP experiments demonstrated that GFP-DGAT2 proteins diffuse in and out of the subdomains that they occupy, and at a rate of mobility comparable to that reported for several other ER subdomain–specific membrane proteins (Nehls et al., 2000; Klopfenstein et al., 2001; Snapp et al., 2003). These latter data indicate that the DGAT-containing subdomains are dynamic regions of the ER and not stable, immobilized aggregates of (transiently overexpressed) protein. Further evidence in support of this conclusion is that Cb5, a membrane protein known to be localized throughout the ER network in plant cells (Hwang et al., 2004), is not excluded from the DGAT1- and DGAT2-containing subdomains (Figure 7), as would be expected if they consisted solely of immobilized aggregates of DGAT proteins.

It is well established that the ER is a functionally complex and dynamic organelle with at least 16 morphologically different membrane domains that carry out a variety of biochemical functions (Staehelin, 1997; Levine and Rabouille, 2005). The enrichment of DGAT proteins in distinct subdomains of the ER suggests that these regions are dedicated to TAG biosynthesis. The existence of focal points for TAG biosynthetic activity would facilitate the separation of metabolic activities that function in membrane lipid and storage oil synthesis, as has been suggested previously (Fernandez and Staehelin, 1987; Vogel and Browse, 1996). However, perhaps the most surprising observation from our microscopic analysis of DGAT1 and DGAT2 is that these proteins do not localize to the same ER subdomains but rather are enriched in different locations within the ER (Figure 7). These data, coupled with data regarding the differential expression of *DGAT1* and *DGAT2* transcripts (Figure 2C) and biochemical differences in their enzymatic activity (Figures 3 and 4), suggest that these two enzymes produce different pools of TAGs within plant cells. Our results do not clarify, however, whether DGAT1 and DGAT2 are actually present in the same cells in developing tung seeds, leaves, or flowers or whether DGAT expression is restricted to different tissue types within these organs. These questions will need to be addressed using monospecific DGAT1 and DGAT2 antibodies and immunomicroscopic analysis of native tung tissues. Regardless, it is tempting to speculate that DGAT1 plays a more general role in TAG metabolism in plant cells, whereas DGAT2 has primarily evolved to accommodate the processing and accumulation of unusual fatty acids. In support of this premise, DGAT1 has been shown to play a role in the production of TAGs during cellular senescence in plants (Kaup et al., 2002), and additional studies in mammals have begun to highlight the existence of a dynamic pool of TAGs in cells associated with the temporary storage of fatty acids rather than the long-term storage of TAGs as a carbon and energy reserve (Murphy, 2001; Liu et al., 2004; Smirnova et al., 2006).

The roles of DGAT1 and DGAT2 in oil production, however, do not have to be mutually exclusive. In some plants, DGAT1 may play a more dominant role depending on gene expression patterns and protein accumulation, whereas in plants containing unusual fatty acids, DGAT2 may play a more important role. Nonetheless, the enrichment of enzymes for unusual fatty acid metabolism into distinct regions of the ER would provide an effective mechanism for excluding the unusual fatty acids from membrane lipids, which otherwise could be disruptive to the structure and/or functioning of the membrane lipid bilayer, and for channeling unusual fatty acids into storage oils.

Biogenesis of DGAT ER Subdomains and Implications for Oilseed Engineering

A major goal is to now determine how the ER subdomains containing DGAT enzymes are formed and what their roles are in storage oil biosynthesis. Toward this end, we investigated the intracellular sorting pathways by which the DGATs are targeted and retained within the ER. Each of the DGAT enzymes is predicted to contain multiple TMDs (Figures 1A, 1B, and 8B); therefore, these proteins are likely inserted cotranslationally into ER membranes by an N-terminal signal anchor (TMD) sequence and the signal recognition particle/Sec61p-dependent pathway (reviewed in Shan and Walter, 2005). Once in the ER, the DGATs must be retained there by either static- or retrieval-mediated mechanisms, and they may contain additional signals for sorting to their respective subdomains. Characterization of the topological orientation of DGAT1 and DGAT2 revealed that the N and C termini of both proteins are exposed on the cytosolic side of ER membranes (Figure 8), and targeting assays with a GFP-Cf9 reporter protein in onion epidermal cells revealed that both DGATs possess at their C terminus a pentapeptide ER retrieval motif (Figure 9) similar to that recently identified in FAD2 enzymes (McCartney et al., 2004). Notably, although the C-terminal ER retrieval motifs of DGAT1 and DGAT2 were sufficient for localizing GFP-Cf9 to the ER (Figure 9), neither signal alone was sufficient for localizing GFP-Cf9 to the subdomains of the ER that contain the full-length DGAT proteins (Figure 10). These data

indicate that although the DGAT C-terminal ER retrieval signals function in steady state localization in the ER, additional portions of the DGAT proteins are required for targeting to their respective ER subdomains.

There are at least two mechanisms by which additional portions of DGAT protein sequence could contribute to the localization of the enzymes in specific ER subdomains. One possibility is that DGAT enzyme activity itself generates a local pool of TAGs and that DGAT enzymes have higher affinity for TAG-enriched regions of the ER membrane compared with the surrounding phospholipid bilayer. These local pools of lipids and DGAT proteins could serve as nucleating centers to attract additional enzymes and proteins (e.g., oleosins) involved in TAG metabolism. Although we did not test directly the localization of inactivated forms of the tung DGAT proteins, we did investigate the functional and cellular properties of the *Arabidopsis* DGAT1 and DGAT2 proteins as well as a modified version of tung DGAT1, specifically a chimera of tung DGAT1 and GFP (GFP-DGAT1). *Arabidopsis* DGAT1 was entirely functional in our yeast complementation assay and, similar to tung DGAT1, was localized to distinct regions of the ER in suspension-cultured plant cells (see Supplemental Figure 8 online). *Arabidopsis* DGAT2, on the other hand, showed no detectable activity in yeast complementation assays (similar to the findings of Lardizabal et al. [2001]) and was not localized to any ER subdomains but rather was found throughout the entire ER network in plant cells (see Supplemental Figure 8 online). These data suggest that the activity of DGAT enzymes is essential for their nucleation and/or targeting to specific subdomains of the ER. However, DGAT enzyme activity alone is not sufficient for targeting to ER subdomains, because GFP-tagged tung DGAT1 (GFP-DGAT1) possessed similar enzymatic activity to that of myc-DGAT1 (see Supplemental Figure 3 online) but was not enriched in any distinct regions of the ER (data not shown). Based on these results, we hypothesize that the addition of GFP to the N terminus of DGAT1 prevents its ability to form homooligomers, which, as discussed below, may be important for its proper localization within the ER.

Another mechanism by which additional portions of DGAT protein sequence contribute to their localization in certain regions of the ER, in addition to a prerequisite for enzyme activity, is through homotypic oligomerization. For instance, there is evidence that the retention of certain proteins within the Golgi occurs by the formation of homooligomers, which prevents further transport to other compartments within the endomembrane system (Nilsson et al., 1994). Similar mechanisms of homotypic oligomerization have been proposed to promote the localization of certain membrane proteins in the ER (Ivessa et al., 1992). Although the oligomerization status of plant DGATs is currently unknown, human DGAT1 forms homotetramers (Cheng et al., 2001). Thus, it is possible that the oligomerization of plant DGAT enzymes could nucleate the formation of dynamic, functional centers within the ER dedicated to TAG biosynthesis. The recruitment of additional interacting proteins, such as other acyltransferases and/or oleosins, could provide additional machinery for the specialized production and packaging of lipids destined for storage oils. Moreover, the inability of DGAT1 and DGAT2 to interact and form heterooligomers would provide a simple mechanism for the spatial segregation of these enzymes (and their putative associated protein complexes) in ER membranes. We are currently testing this hypothesis by investigating the ability of DGAT1 and DGAT2 to interact through yeast two-hybrid split-ubiquitin screening (Thaminy et al., 2004). Notably, recent characterization of an *Arabidopsis* LPAT enzyme revealed that this protein is also enriched in certain regions of the ER (Kim et al., 2005), and we are also determining whether these regions are equivalent to those containing DGAT1 and/or DGAT2.

Overall, the functional and cellular aspects of DGATs presented here have at least two important implications for the genetic engineering of crop plants that are tailored for the production of industrially important oils. First, it is clear from these studies that coexpression of DGAT2 and an enzyme responsible for the synthesis of an unusual fatty acid from the same species is likely to lead to an enhanced accumulation of this fatty acid in a transgenic host. This hypothesis is supported by the observation that co-overexpression of castor bean *DGAT2*, but not *Arabidopsis DGAT2*, with castor oleate hydroxylase (van de Loo et al., 1995) leads to substantial increases in hydroxy fatty acid content in *Arabidopsis* seed lipids (i.e., a 50 to 70% increased overexpression of oleate hydroxylase alone) (J.M. Shockey and J. Browse, unpublished data). Second, the optimal production of storage oils containing unusual fatty acids may be dependent on the ability of the expressed proteins to establish functional ER subdomains that are dedicated to the production of specific types of TAGs. The molecular mechanisms underlying the formation of these subdomains and their protein composition are the subject of future investigation.

METHODS

Recombinant DNA Procedures and Reagents

Standard recombinant DNA procedures were performed as described by Sambrook et al. (1989). Molecular biology reagents were purchased from New England Biolabs, Promega, Perkin-Elmer, Stratagene, or Invitrogen. Oligonucleotides were synthesized by either University of Guelph Laboratory Services or Invitrogen. DNA was isolated and purified using reagents from Qiagen and Promega. All DNA constructs were sequenced using dye-terminated cycle sequencing to verify that undesirable mutations were not introduced during amplification or cloning procedures. Mutagenesis was performed using appropriate complementary forward and reverse mutagenic primers and the QuikChange site-directed mutagenesis kit according to the manufacturer's instructions (Stratagene). Complete details of the oligonucleotide primers used in the gene cloning and plasmid constructions described below are available upon request.

Several conserved regions of the DGAT families identified previously served as starting points for the identification of tung (*Vernicia fordii*) *DGAT1* and *DGAT2* genes (Hobbs et al., 1999; Lardizabal et al., 2001). Sense-strand degenerate oligonucleotide primers were designed to the amino acid sequences -QSHAGLFNL- and -GYEPHSVLP-, which span residues 130 to 138 and 106 to 114 of *Arabidopsis thaliana* DGAT1 and DGAT2, respectively. Paired with a capped oligo(dT) primer, PCRs with tung seed cDNA library (Dyer et al., 2002a) λDNA preparations yielded amplicons corresponding to the 3′ ends of both DGAT cDNAs. Attempts at isolation of the remaining 5′ cDNA ends from the seed cDNA library were unsuccessful. The 5′ sequence of tung *DGAT1* was determined through multiple rounds of adaptor-anchored PCR from tung genomic DNA (Universal GenomeWalker kit; Clontech). Genomic sequences were

compared with the cDNA sequence of *Arabidopsis* DGAT1 until a putative start Met ATG codon was found. Genomic PCR and RT-PCR (Superscript III first-strand cDNA synthesis kit; Invitrogen) results were compared to determine the 5′ untranslated region for DGAT1. The complete sequence for tung *DGAT2* was determined by 5′ rapid amplification of cDNA ends (5′ RACE system; Invitrogen) using capped oligo(dT)-primed total RNA isolated from developing tung seeds. Finally, PCR products encompassing the full-length open reading frames (ORFs) were amplified, digested, and cloned into the pYes3-CT vector (Invitrogen) for expression in *Saccharomyces cerevisiae*.

Yeast and plant expression plasmids containing the tung DGAT1 or DGAT2 ORFs were constructed as follows. First, the tung DGAT1 and DGAT2 ORFs were amplified from pYes3-CT/DGAT1 and pYes3-CT/DGAT2 using PCR with appropriate forward and reverse primers that introduced in-frame *Xba*I or *Bam*HI sites 5′ and 3′ of the start and stop codons of DGAT1 and DGAT2, respectively. Next, PCR products were gel-purified and subcloned into either *Xba*I- or *Bam*HI-digested pRTL2/mycX, a modified version of the plant expression vector pRTL2ΔN/S (Lee et al., 1997) that includes the 35S cauliflower mosaic virus promoter and sequences encoding an initiator Met, Gly linkers, and the myc epitope tag (underlined: MGEQKLISEEDLG-) (Fritze and Anderson, 2000) followed by in-frame *Xba*I and *Bam*HI sites. The resulting plasmids were referred to as pRTL2/myc-DGAT1 and pRTL2/myc-DGAT2. pRTL2/GFP-DGAT2 was generated by ligating the *Bam*HI fragment from pRTL2/myc-DGAT2 into *Bam*HI-digested pRTL2/monoGFP-MCS, a plasmid containing a modified version of the GFP, in which the Leu at position 221 in the GFP ORF was mutated (via site-directed mutagenesis) to Lys. This modification to GFP disrupts the protein's dimerization domain (Zacharias et al., 2002) and helps to prevent alterations in the target membrane (e.g., aggregation) attributable to transient (over)expression of the membrane-bound GFP fusion protein (Lisenbee et al., 2003). pRTL2-HA-DGAT2 was constructed by replacing in pRTL2/myc-DGAT2 (via site-directed mutagenesis) sequences encoding the myc epitope tag with a HA epitope tag (underlined: MGYPYDVPDYAG-) (Fritze and Anderson, 2000). To construct pRTL2/DGAT1-myc and pRTL2/DGAT2-myc, the DGAT1 and DGAT2 ORFs were amplified using PCR and pRTL2/myc-DGAT1 and pRTL2/myc-DGAT2, respectively, as template DNA. Forward and reverse primers used in these PCRs introduced an in-frame *Xba*I site 5′ of the DGAT1 or DGAT2 start codon and a *Nco*I site 3′ of each ORF. The resulting PCR products were digested with *Xba*I and *Nco*I and ligated into *Xba*I-*Nco*I–digested pRTL2/X-myc, a modified version of pRTL2ΔN/S with sequences encoding *Xba*I, *Nhe*I, and *Nco*I sites followed by a myc epitope tag and a stop codon. Construction of pRTL2/myc-Cb5, encoding an N-terminal myc-tagged version of the A isoform of tung Cb5, has been described (Hwang et al., 2004).

The yeast expression plasmid containing *Arabidopsis* DGAT1 (AtDGAT1) was generated as follows. An amplicon representing the At DGAT1 ORF was generated using gene-specific primers and *Pfu* Ultra (Stratagene). The template for this PCR was first-strand cDNA generated from developing *Arabidopsis* silique total RNA using Superscript III reverse transcriptase (Invitrogen). PCR products were T-tailed and cloned into the yeast expression plasmid pYes2.1 TOPO as described by the manufacturer (Invitrogen). pYes2.1/AtDGAT2 was generated by amplification of the *Arabidopsis* DGAT2 (AtDGAT2) ORF from ABRC clone U16101 (Newman et al., 1994), followed by T-tailing and cloning into pYes2.1 TOPO, as described above. Plant expression plasmids containing myc epitope–tagged versions of *Arabidopsis* DGAT1 or DGAT2 were constructed as follows. First, the *Arabidopsis* DGAT1 and DGAT2 ORFs were amplified from pYes2.1/AtDGAT1 and pYes2.1/AtDGAT2 using PCR with appropriate forward and reverse primers that introduced in-frame *Xba*I or *Bam*HI sites 5′ and 3′ of the start and stop codons of At DGAT1 and At DGAT2, respectively. Next, PCR products were gel-purified, subcloned into pCR2.1 TOPO, and then cloned into either *Xba*I- or *Bam*HI-digested pRTL2/mycX.

Plasmids coding for GFP-Cf9 mutants with altered amino acid residues at the C terminus of Cf9 (Figure 9) were constructed using site-directed mutagenesis and pRTL2/GFP-Cf9 or pRTL2/GFP-Cf9-KKΔNN (McCartney et al., 2004) as template DNA. pRTL2/RFP-HDEL encoding the RFP fused to the N-terminal *Arabidopsis* chitinase signal sequence and the C-terminal HDEL retrieval signal was constructed by amplifying (via PCR) sequences coding the chitinase signal sequence from pBIN/mGFP5-HDEL (provided by Jim Haseloff, University of Cambridge) (Haseloff et al., 1997) along with 5′ and 3′ *Nco*I sites. The resulting PCR products were digested with *Nco*I and ligated into *Nco*I-digested pRTL2/MCS-RFP-stop. Next, sequences in the RFP 3′ untranslated region and stop codon were modified (via site-directed mutagenesis) to encode a C-terminal HDEL and stop codon. pRTL2/MCS-RFP-stop was generated by amplifying an ORF encoding the monomeric RFP from pmRFPC1 (provided by Ray Truant, McMaster University, Hamilton, Ontario, Canada) (Irwin et al., 2005) using PCR and appropriate forward and reverse primers that introduced in-frame *Xma*I and *Nco*I sites at the 5′ end of RFP and a *Xba*I site at the 3′ end of RFP. The resulting PCR products were then digested with *Xma*I and *Xba*I and ligated into *Xma*I-*Xba*I–digested pRTL2ΔN/S. The resulting plasmid (pRTL2/MCS-RFP *Nco*I-stop) was further modified (via site-directed mutagenesis) to remove a *Nco*I site in the RFP ORF, yielding pRTL2/MCS-RFP-stop. To construct pRTL2/RFP-Rac3, sequences encoding *Arabidopsis* RhoGTPase Rac3 were amplified from pBT4-35S-GFP-Rac3(Q68L) (provided by Arthur Molendijk, Max Planck Institute, Koln, Germany) (Bischoff et al., 2000) using PCR and forward and reverse primers that introduced in-frame *Bgl*II and *Xba*I sites at the 5′ and 3′ ends of RFP, respectively. The resulting PCR products were then digested with *Bgl*II and *Xba*I and ligated into *Bgl*II-*Xba*I–digested pRTL2/RFP-MCS. pRTL2/RFP-MCS was generated by amplifying the RFP ORF from pmRFPC1 using PCR and appropriate forward and reverse primers that introduced an in-frame *Xma*I site at the 5′ end of RFP and *Bgl*II, *Sac*I, and *Xba*I sites at the 3′ end of RFP. The resulting PCR products were then digested with *Xma*I and *Xba*I and ligated into *Xma*I-*Xba*I–digested pRTL2ΔN/S, yielding pRTL2/RFP-MCS. pRTL2/RFP-BS14a encoding RFP fused to the N terminus of the *Arabidopsis* Golgi-localized soluble *N*-ethylmaleimide–sensitive factor attachment protein receptor BS14a (Uemura et al., 2004) was constructed by ligating the *Bam*HI-*Xba*I fragment from pRTL2/GFP-BS14a (McCartney et al., 2005) into *Bgl*II-*Xba*I–digested pRTL2/RFP-MCS.

The myc epitope–tagged yeast expression constructs pYes3-CT/mycDGAT1 and pYes3-CT/myc-DGAT2 were generated by amplification of the ORFs from pRTL2/myc-DGAT1 and pRTL2/myc-DGAT2 (described above) with primers that added *Kpn*I and *Xho*I sites to the 5′ and 3′ ends, respectively. After restriction digestion and gel purification, the products were ligated into pYes3-CT (Invitrogen) cut with the same two enzymes. The GFP-tagged DGAT2 yeast expression vector was constructed by digesting plasmid pRTL2/GFP-DGAT2 with *Kpn*I and *Xho*I to liberate the GFP-DGAT2 ORF and then ligating the gel-purified products into similarly digested pYes3-CT. To generate the GFP-tagged DGAT1 expression vector, a unique *Nhe*I site was first introduced into the polylinker of pYes3-CT by subcloning overlapping, annealed oligonucleotides into the *Eco*RI-*Xho*I sites to produce plasmid pYes3-Nhe. The vector pRTL2-GFPXba-DGAT1 was partially digested with *Kpn*I and *Xba*I to liberate the GFP-tagged DGAT1 ORF, and a fragment of the expected size was gel-purified and ligated into *Kpn*I-*Nhe*I–digested pYES3-Nhe to give plasmid pYes3-GFP-DGAT1.

Plant Material and Determination of Seed Oil Content

Tung fruits, which are produced once per year during the summer months, were collected from the American Tung Oil Corporation orchard in Lumberton, Mississippi, beginning in mid June. This was ~9 weeks

after full bloom and 1 month before the initiation of storage oil synthesis. Seeds were excised and hand-shelled, and kernels were immediately frozen in liquid N_2, then stored at –80°C. Tung oil was extracted from kernels according to the method of Chang et al. (1994) using a Tissuemizer (Tekmar). The ratio of kernel to petroleum ether was 1 g:10 mL. For analysis of eleostearic acid content, methyl esters of extracted oil were prepared using potassium methoxide (Christie et al., 1984), then fatty acid methyl esters (FAMEs) were purified using a 3-mL Accubond solid-phase extraction column containing 200 mg of Alumina N (J&W Scientific) and evaporated to dryness under a nitrogen stream. The residue was resuspended in 1 mL of 10% isopropanol in *n*-hexane containing methyl heptadecanoate as an internal standard. GC analyses were performed on a Hewlett-Packard 5890 series II gas chromatograph (Agilent) equipped with flame ionization detection (FID) and a Supelco SP-2380 column (Sigma-Aldrich). Helium was used as the carrier gas at a flow rate of 8 mL/min. The inlet and detector were held at 200°C. The column oven was temperature programmed from 110 to 160°C at 17°C/min, then to 175°C at 5°C/min, and finally to 200°C at 20°C/min and held for 3 min. Data were collected and processed using the Hewlett-Packard 3365 series II ChemStation.

Genomic DNA Gel Blotting and Gene Expression Analysis

Tung *DGAT* gene structure and genomic copy number were analyzed by DNA gel blotting using nonradioactive DIG-containing probes generated by PCR (PCR DIG probe synthesis kit; Roche Diagnostics) as described by Shockey et al. (2005). Total RNA was extracted from tung leaves, flowers, and developing seeds using the hot borate method of Wan and Wilkins (1994). Twenty micrograms of total RNA was separated on MOPS–formaldehyde agarose gels and transferred to membranes after 30 min of incubation in 10× SSC (1× SSC is 0.15 M NaCl and 0.015 M sodium citrate) to remove excess formaldehyde. RNA gel blots were then hybridized, washed, and developed as described for DNA gel blotting (Shockey et al., 2005). A LAS-1000Plus digital imaging system (Fuji Medical Systems) was used for signal visualization, digital data capture, and quantification.

Yeast Strains, Cell Culturing, and Extraction of Lipids

Yeast strains SCY325 (*MAT*α, *ade2-1*, *trp1-1*, *can1-100*, *leu2-3,112*, *ura3-1*, and *his3-11,15*) and SCY1998 (*MAT*α, *lro1*Δ*::LEU2*, *dga1*Δ*::URA3*, *ade2-1*, *trp1-1*, *can1-100*, *leu2-3,112*, *ura3-1*, and *his3-11,15*) were used throughout these studies (Oelkers et al., 2002). Yeast cells were maintained on YPD plates (1% yeast extract [w/v], 2% peptone [w/v], and 2% dextrose [w/v]) solidified with 2% agar (w/v). Cells were transformed using the lithium acetate procedure of Gietz and Woods (1994), and transformants were selected by growth on synthetic dextrose medium (2% dextrose [w/v] and 0.67% yeast nitrogen base without amino acids [w/v]) containing appropriate auxotrophic supplements (Bufferad). Single colonies were inoculated into liquid synthetic dextrose medium and cultured overnight at 30°C and 300 rpm in an orbital shaker. The OD_{600} of the culture was determined, an appropriate volume of cell culture was harvested by centrifugation, and cells were resuspended in synthetic galactose medium (2% galactose [w/v], 0.67% yeast nitrogen base without amino acids [w/v], and appropriate auxotrophic supplements) at an OD_{600} of 0.4. Cultures were supplemented with 0.1% tung oil (v/v) and 1 mg/mL *Candida rugosa* lipase (Sigma-Aldrich). Cells were incubated for 20 to 22 h at 30°C and 300 rpm, harvested by centrifugation, and then washed once with 1% Tween 40 (w/v) and twice with deionized water. Cells were lysed, and lipids were extracted using the method of Bligh and Dyer (1959). All organic solvents contained 0.01% butylated hydroxytoluene as an antioxidant, and samples were maintained under reduced light and a nitrogen atmosphere to minimize oxidation of eleostearic acid.

Analysis of Lipids by TLC, GC-FID, HPLC-PDA, and LC-MS

TLC was performed as described (Dyer et al., 2002b). Briefly, lipid samples were spotted onto silica gel plates and then separated using a mobile phase of hexane:diethyl ether:glacial acetic acid (80:20:1, v/v/v). Lipid spots were visualized by charring and identified by comparison with retention factor values of lipid standards (TLC Mix 34; Larodan).

GC with FID was also performed as described (Dyer et al., 2002b). Briefly, FAMEs were prepared using sodium methoxide in methanol, and methyl heptadecanoate was used as an internal standard. FAMEs were analyzed on an Agilent 6890N gas chromatograph and identified by comparison of relative retention times with FAME standards. Percentages of each FAME were calculated based on total FAME area counts. Details regarding the extraction and analysis of oil from developing tung seeds are provided above.

For HPLC-PDA analysis, 1 mg of yeast lipid extract was reduced to ~50 μL, 450 μL of mobile phase (acetonitrile:isopropanol, 70:30) was added, and samples were filtered through glass wool. Lipids were analyzed on a Waters HPLC system equipped with a model 600E multisolvent delivery system, a model 712 WISP autosampler, and a model 996 photodiode array detector. The separation was performed on a Waters Nova-Pak C18 column (300 × 3.9 mm, 60 Å, 4 μm). The mobile phase flow rate was 1.0 mL/min. Solvents were sparged with helium at a flow rate of 30 mL/min. HPLC-PDA data were analyzed using the Millennium^{32} version 4.0 software package (Waters). TAGs were identified by comparison of peak retention times with those of lipid standards run on the same instrument. Lipid standards containing eleostearic acid were generated by lipase-catalyzed transesterification of tung oil with palmitic, stearic, oleic, linoleic, or linolenic acid as described (Ramírez Fajardo et al., 2003), TAGs resulting from each reaction were separated by HPLC, and fractions were collected. The fatty acid composition of each TAG peak was determined by GC-FID.

Yeast lipids were also analyzed by LC-MS with atmospheric pressure chemical ionization (APCI) and collision-induced dissociation, as described previously (Bland et al., 2004). Instrumentation included a Waters Alliance 2695 HPLC apparatus equipped with a column heater, a model 996 photodiode array detector, and a Waters Micromass ZMD mass spectrometer. The ZMD mass spectrometer was equipped with an APCI source and parameters set as follows: corona voltage, 3.5 kV; cone voltage, 30 V; source block temperature, 125°C; APCI heater, 500°C; desolvation gas, 450 liters/min; cone gas, 100 liters/min; scan range, *m/z* 250 to 1000. Columns included a silica column (4.6 × 250 mm, 10 μm; Alltech) or two Luna C18 columns (2.0 × 50 mm, 3 μm; Phenomenex) in series, heated to 30°C. Lipid analysis was performed on chloroform solutions of ~6 mg/mL. Normal phase analyses were performed on 20-μL injections with a 10-min gradient from 1% ether in hexane to 10% ether followed by a 2 min hold and an 8-min gradient to 25% ether, at a flow rate of 1 mL/min. Reverse-phase analyses were performed on 10-μL injections using a program of 10 min of isocratic methanol followed by a 20-min gradient of 0 to 25% methylene chloride in methanol, at a flow rate of 0.3 mL/min. In addition to the MH^+ value found for each TAG species in the APCI-MS spectra, fragmentation peaks corresponding to the loss of the *sn*-1 and *sn*-3 fatty acids were also observed (Kusaka et al., 1996). The fragmentation was increased with in-source collision-induced dissociation, causing the 2-monoacylglycerol fragment to become more prominent. Although this method provided clear identification of the fatty acid composition of each TAG species (see Supplemental Figure 1 online), poor fragmentation of eleostearoyl-containing TAGs prevented the stereospecific assignment of fatty acyl side chains.

Yeast Extract Preparation and in Vitro DGAT Enzyme Assay

Yeast cells (strain SCY1998) harboring galactose-inducible *DGAT1* or *DGAT2* genes were grown in liquid synthetic galactose medium lacking

Trp, and cells were harvested by centrifugation. The cell pellets were suspended in cell-breaking buffer I (1× PBS containing dissolved Complete Mini EDTA-free protease cocktail tablets [Roche Diagnostics]; 1 tablet/10 mL buffer]) and lysed in 12-mL glass tubes by vortexing in an equal volume of acid-washed 600-μm glass beads (5 × 1 min), followed by centrifugation at 1500*g* for 15 min to remove cellular debris and unbroken cells. The supernatants from the low-speed spin were centrifuged at 100,000*g* for 1 h at 4°C. The resulting microsomal membrane pellets were resuspended in 50 mM Tris-HCl and 25% glycerol, pH 8.0, divided into aliquots, and frozen at –80°C. DGAT enzyme activity was measured by in vitro assay (Zou et al., 1999) containing 100 μM Tris-HCl, pH 8.0, 400 μM diacylglycerol (delivered from a 40 mM stock in methanol), 20 μM [1-^{14}C]acyl-CoA (specific activity, 20,000 cpm/μmol; prepared enzymatically as described by Rajasekharan et al. [1993]), and 25 μg of yeast microsomal membrane protein in a total volume of 100 μL. The mixture was incubated at 30°C for 1 h and then extracted twice with 400 μL of hexane:isopropanol (3:2, v/v) (Milcamps et al., 2005). The upper hexane phases were pooled, dried under N_2, redissolved in a small volume of chloroform containing 200 μg of carrier trilinolein, and chromatographed on silica gel TLC plates using *n*-hexane:diethyl ether:acetic acid (80:20:1, v/v) as the mobile phase. TAG spots (retention factor = 0.30) were visualized by light staining with iodine vapor and scraped, and radioactivity was quantified by liquid scintillation counting. Each enzyme was tested in triplicate with each combination of substrates. Each enzyme/acyl-CoA combination was also tested in triplicate with no exogenous DAG. The average value of the samples not containing exogenous DAG was subtracted from the average values of the other assays before plotting the data.

Transient Transformation of Tobacco BY-2 and Onion Epidermal Cells and Fluorescence Microscopy

Tobacco (*Nicotiana tabacum* cv BY-2) suspension-cultured cells were maintained and prepared for biolistic bombardment as described previously (Banjoko and Trelease, 1995). Briefly, transient transformations were performed using 5 μg of plasmid DNA (or 2.5 μg of each plasmid for cotransformations) with a biolistic particle delivery system 1000/HE (Bio-Rad Laboratories). Bombarded cells were incubated for 4 h to allow for expression and sorting of the introduced gene product(s), fixed in formaldehyde, incubated with 0.01% (w/v) pectolyase Y-23 (Kyowa Chemical Products), and permeabilized with either 0.3% Triton X-100 (v/v) or 25 μg/mL digitonin (Sigma-Aldrich) (Lee et al., 1997). Cells were evaluated after 4 h to ensure that any potential negative effects attributable to (membrane) protein overexpression were diminished. Antibodies and sources were as follows: mouse anti-myc antibodies in hybridoma medium (clone 9E10; Princeton University Monoclonal Antibody Facility); rabbit anti-castor bean calnexin (Coughlan et al., 1997); mouse anti-tubulin (Sigma-Aldrich); rabbit anti-myc and mouse anti-HA (Bethyl Laboratories); goat anti-mouse Alexa Fluor 488 IgGs, goat anti-mouse Cy5, and goat anti-rabbit Cy5 (Cedar Lane Laboratories); and goat anti-rabbit rhodamine red-X IgGs (Jackson ImmunoResearch Laboratories). ConA conjugated to Alexa 594 (Molecular Probes) was added to BY-2 cells at a final concentration of 5 μg/mL during the final 20 min of incubation with secondary antibodies. All antibodies, with the exception of anti-calnexin antibodies, were IgG-affinity purified using protein A–Sepharose columns.

Transient transformation of onion (*Allium cepa*) epidermal cells was performed as described by McCartney et al. (2004). Onions were purchased at a local greengrocer in Guelph, Canada, and bombardments were performed with 10 μg of plasmid DNA or 5 μg of each plasmid for cotransformations. Approximately 8 h after bombardment, peels were mounted onto glass slides without a cover slip, and GFP and RFP signals were analyzed via fluorescence microscopy.

Epifluorescent images of BY-2 and onion cells were acquired using a Zeiss Axioskop 2 MOT epifluorescence microscope (Carl Zeiss) with a Zeiss 63× Plan Apochromat oil-immersion objective. Image capture was performed using a Retiga 1300 charge-coupled device camera (Qimaging) and Northern Eclipse 5.0 software (Empix Imaging). CLSM images of BY-2 cells were acquired using a Leica DM RBE microscope with a Leica 63× Plan Apochromat oil-immersion objective, a Leica TCS SP2 scanning head, and the Leica TCS NT software package (version 2.61). Fluorophore emissions were collected sequentially in double- and triple-labeling experiments; single-labeling experiments showed no detectable crossover at the settings used for data collection. Confocal images were acquired as a z-series of representative cells, and single optical sections were saved as 512- × 512-pixel digital images. All fluorescence images of cells shown in the figures are representative of >50 independent (transient) transformations from at least two independent transformation experiments. Figure compositions were generated using Adobe Photoshop CS (Adobe Systems).

Qualitative FRAP experiments were performed using the Leica CLSM apparatus and the 63× oil-immersion objective lens described above and methods adapted from Brandizzi et al. (2002) and Snapp et al. (2003). Measurements of prebleach and postbleach signals, modulations of laser light intensity, and time-lapse scanning were all performed using the Leica TCS NT software package (version 2.61). For the quantification of fluorescence, signals from an entire cell were sampled (512 × 512 pixels) using low-intensity illumination (16% transmittance of the 488-nm laser line) at time intervals of either 2 s before the bleach treatment (generally, 5 data points) or 5 s after the bleach treatment (generally, 10 data points), followed by 10 s up to 3 min after bleach. Photobleaching was accomplished by scanning with high-intensity illumination (80% transmittance) for 6 s and zooming into a selected region of the cell at 32× zoom. For all experiments, the size of the bleached region of interest was 5 to 6 μm^2. Fluorescence recovery curves were generated by normalizing the postbleach fluorescence intensities to the prebleached signal scaled to 100% and after subtraction of the background signal. The half-time in florescence recovery of a GFP chimera protein was calculated as the time required for fluorescence in the photobleached region to recover to 50% of the final recovered intensity.

Phylogenetic Analysis

The encoded protein sequences of known and putative DGAT genes were aligned (see Supplemental Figure 9 online) using the ClustalX program (version 1.81; Thompson et al., 1997) using default settings. Phylogenetic trees were created in Phylip format and bootstrapped using a random number generator seed of 111 and 1000 bootstrap trials. The dendrogram was displayed graphically using the TreeView program (version 1.6.6; Page, 1996).

Accession Numbers

The GenBank/EMBL accession numbers for cDNAs (or genes) described in this study are as follows: *Arabidopsis DGAT1* (AJ131831) and *DGAT2* (T45783); *Arabidopsis* RhoGTPase *Rac3* (AF031427); *Brassica napus DGAT1* (AF164434) and *DGAT2* (AF155224); *Cladosporium fulvum-9* disease resistance gene product (CAA05274); human *DGAT1* (NM_012079) and *DGAT2* (AF384163); *S. cerevisiae DGA1* (YOR245C); tobacco *DGAT1* (AF129003); tung *Cb5A* (AY578727); tung *DGAT1* cDNA (DQ356680) and *DGAT2* cDNA (DQ356682); and tung genomic *DGAT1* (DQ356679) and *DGAT2* (DQ356681). Additional sequences included in the dendrogram in Figure 1 represent predicted proteins derived from EST contig assemblies obtained from the Plant Gene Indices database at The Institute for Genomic Research (http://www.tigr.org/tdb/tgi/plant.shtml). These sequences include cotton (*Gossypium hirsutum*) *DGAT2* (TC28496), rice (*Oryza sativa*) *DGAT1* (TC251130) and *DGAT2* (TC252055), soybean (*Glycine max*) *DGAT1* (TC231740), and wheat (*Triticum aestivum*) *DGAT2* (TC208469).

Supplemental Data

The following materials are available in the online version of this article.

Supplemental Figure 1. Comparison of HPLC-PDA Profiles of Yeast and Tung Oil Triglycerides.

Supplemental Figure 2. Identification of TAGs by LC-MS.

Supplemental Figure 3. Comparison of Native, myc-Tagged, and GFP-Tagged DGAT1 and DGAT2 Activities in Yeast Cells.

Supplemental Figure 4. Subcellular Localization of DGAT1 and DGAT2 in Tobacco BY-2 Cells.

Supplemental Figure 5. Subcellular Localization of Coexpressed myc-DGAT1 and HA-DGAT2 in Tobacco BY-2 cells.

Supplemental Figure 6. Subcellular Localization of DGAT1, DGAT2, and Calnexin in Tobacco BY-2 Cells.

Supplemental Figure 7. Colocalization of GFP-Cf9-DGAT2 and GFP-Cf9-DGAT2+13 with the Golgi Marker Protein RFP-BS14a in Onion Epidermal Cells.

Supplemental Figure 8. Functional and Cellular Analysis of *Arabidopsis* DGAT1 and DGAT2.

Supplemental Figure 9. Alignment of DGAT1 and DGAT2 Protein Sequences.

ACKNOWLEDGMENTS

We thank Sean Coughlan for providing anti-calnexin antibodies, Ray Truant, Jim Haseloff, and Arthur Molenjijk for pmRFPC1, pBIN/mGFP5-HDEL, and pBT-35S-GFP-Rac3(Q68L), respectively, and Steven Sturley for the yeast strains SCY325 and SCY1998. We also thank Federica Brandizzi and Peter Kim for their advice with photobleaching experiments. Jeffrey Cary, Yeen Ting Hwang, Hyun-Uk Kim, Andrew McCartney, and Judy Schnurr are thanked for their critical comments during the writing of the manuscript. This work was supported by the U.S. Department of Agriculture, Agricultural Research Service (Current Research Information System project numbers 6435-41000-083-00D to J.M.S., D.C.C., J.-C.K., and J.M.D., 6435-41000-510-01 to J.M.B., and 6435-41000-087-02S to R.T.M.), the Ontario Research and Development Challenge Fund (Ontario Centre for Agriculture Genomics Grant 046061 to S.J.R), the Natural Sciences and Engineering Research Council (Grant 217291 to R.T.M.), and the Ontario Premier's Research in Excellence Award (to R.T.M).

Received April 25, 2006; revised June 14, 2006; accepted July 25, 2006; published August 18, 2006.

REFERENCES

Banjoko, A., and Trelease, R.N. (1995). Development and application of an *in vivo* plant peroxisome import system. Plant Physiol. **107,** 1201–1208.

Benghezal, M., Wasteneys, G.O., and Jones, D.A. (2000). The C-terminal dilysine motif confers endoplasmic reticulum localization to type I membrane proteins in plants. Plant Cell **12,** 1179–1201.

Bischoff, F., Vahlkamp, L., Molendijk, A., and Palme, K. (2000). Localization of AtROP4 and AtROP6 and interaction with the guanine nucleotide dissociation inhibitor AtRhoGDI1 from Arabidopsis. Plant Mol. Biol. **42,** 515–530.

Bland, J.M., Park, Y.I., Raina, A.K., Dickens, J.C., and Hollister, B. (2004). Trilinolein identified as a sex-specific component of tergal glands in alates of *Coptotermes formosanus.* J. Chem. Ecol. **30,** 835–849.

Bligh, E.G., and Dyer, W.J. (1959). A rapid method of total lipid extraction and purification. Can. J. Biochem. Physiol. **37,** 911–917.

Bouvier-Navé, P., Benveniste, P., Oelkers, P., Sturley, S.L., and Schaller, H. (2000). Expression in yeast and tobacco of plant cDNAs encoding acyl CoA:diacylglycerol acyltransferase. Eur. J. Biochem. **267,** 85–96.

Brandizzi, F., Snapp, E.L., Roberts, A.G., Lippincott-Schwartz, J., and Hawes, C. (2002). Membrane protein transport between the endoplasmic reticulum and the Golgi in tobacco leaves is energy dependent but cytoskeleton independent: Evidence from selective photobleaching. Plant Cell **14,** 1293–1309.

Cao, Y., and Huang, A.H.C. (1986). Diacylglycerol acyltransferase in maturing oil seeds of maize and other species. Plant Physiol. **82,** 813–820.

Cases, S., Smith, S.J., Zheng, Y.W., Myers, H.M., Lear, S.R., Sande, E., Novak, S., Collins, C., Welch, C.B., Lusis, A.J., Erickson, S.K., and Farese, R.V., Jr. (1998). Identification of a gene encoding an acyl CoA:diacylglycerol acyltransferase, a key enzyme in triacylglycerol synthesis. Proc. Natl. Acad. Sci. USA **95,** 13018–13023.

Cases, S., Stone, S.J., Zhou, P., Yen, E., Tow, B., Lardizabal, K.D., Voelker, T., and Farese, R.V., Jr. (2001). Cloning of DGAT2, a second mammalian diacylglycerol acyltransferase, and related family members. J. Biol. Chem. **276,** 38870–38876.

Chang, M.-K., Conkerton, E.J., Chapital, D., and Wan, P.J. (1994). Behavior of diglycerides and conjugated fatty acid triglycerides in reverse-phase chromatography. J. Am. Oil Chem. Soc. **71,** 1173–1175.

Cheng, D., Meegalla, R.L., He, B., Cromley, D.A., Billheimer, J.T., and Young, P.R. (2001). Human acyl-CoA:diacylglycerol acyltransferase is a tetrameric protein. Biochem. J. **359,** 707–714.

Christie, W.W., Connor, K., and Noble, R.C. (1984). Preparative separation of milk fatty acid derivatives by high-performance liquid chromatography. J. Chromatogr. **298,** 513–515.

Coughlan, S.J., Hastings, C., and Winfrey, R. (1997). Cloning and characterization of the calreticulin gene from *Ricinus communis* L. Plant Mol. Biol. **34,** 897–911.

Dahlqvist, A., Ståhl, U., Lenman, M., Banas, A., Lee, M., Sandager, L., Ronne, H., and Stymne, S. (2000). Phospholipid:diacylglycerol acyltransferase: An enzyme that catalyzes the acyl-CoA-independent formation of triacylglycerol in yeast and plants. Proc. Natl. Acad. Sci. USA **97,** 6487–6492.

Dyer, J.M., Chapital, D.C., Kuan, J.-C., Mullen, R.T., Turner, C., McKeon, T.A., and Pepperman, A.B. (2002a). Molecular analysis of a bifunctional fatty acid conjugase/desaturase from tung. Implications for the evolution of plant fatty acid diversity. Plant Physiol. **130,** 2027–2038.

Dyer, J.M., Chapital, D.C., Kuan, J.W., Mullen, R.T., and Pepperman, A.B. (2002b). Metabolic engineering of *Saccharomyces cerevisiae* for production of novel lipid compounds. Appl. Microbiol. Biotechnol. **59,** 224–230.

Dyer, J.M., Chapital, D.C., Kuan, J.-C.W., Shepherd, H.S., Tang, F., and Pepperman, A.B. (2004). Production of linolenic acid in yeast cells expressing an omega-3 desaturase from tung (*Aleurites fordii*). J. Am. Oil Chem. Soc. **81,** 647–651.

Dyer, J.M., and Mullen, R.T. (2005). Development and potential of genetically engineered oilseeds. Seed Sci. Res. **15,** 255–267.

Fernandez, D.E., and Staehelin, L.A. (1997). Does gibberellic acid induce the transfer of lipase from protein bodies to lipid bodies in barley aleurone cells? Plant Physiol. **85,** 487–496.

Fritze, C.E., and Anderson, T.R. (2000). Epitope tagging: General method for tracking recombinant proteins. Methods Enzymol. **327,** 3–16.

Gietz, R.D., and Woods, R.A. (1994). High efficiency transformation of yeast. In Molecular Genetics of Yeast: Practical Approaches, J.A. Johnston, ed (New York: Oxford University Press), pp. 121–134.

Haseloff, J., Siemering, K.R., Prasher, D.C., and Hodge, S. (1997). Removal of a cryptic intron and subcellular localization of green fluorescent protein are required to mark transgenic Arabidopsis plants brightly. Proc. Natl. Acad. Sci. USA **94,** 2122–2127.

He, X., Chen, G.Q., Lin, J.T., and McKeon, T.A. (2004a). Regulation of diacylglycerol acyltransferase in developing seeds of castor. Lipids **39,** 865–871.

He, X., Turner, C., Chen, G.Q., Lin, J.T., and McKeon, T.A. (2004b). Cloning and characterization of a cDNA encoding diacylglycerol acyltransferase from castor bean. Lipids **39,** 311–318.

Hobbs, D.H., Lu, C., and Hills, M.J. (1999). Cloning of a cDNA encoding diacylglycerol acyltransferase from *Arabidopsis thaliana* and its functional expression. FEBS Lett. **452,** 145–149.

Hwang, Y.T., Pelitire, S.M., Henderson, M.P., Andrews, D.W., Dyer, J.M., and Mullen, R.T. (2004). Novel targeting signals mediate the sorting of different isoforms of the tail-anchored membrane protein cytochrome b_5 to either endoplasmic reticulum or mitochondria. Plant Cell **16,** 3002–3019.

Ichihara, K., Takahashi, T., and Fujii, S. (1988). Diacylglycerol acyltransferase in maturing safflower seeds: Its influences on the fatty acid composition of triacylglycerol and on the rate of triacylglycerol synthesis. Biochim. Biophys. Acta **958,** 125–129.

Irwin, S., Vandelft, M., Pinchev, D., Howell, J.L., Graczyk, J., Orr, H.T., and Truant, R. (2005). RNA association and nucleocytoplasmic shuttling by ataxin-1. J. Cell Sci. **118,** 233–242.

Ivessa, N.E., De Lemo-Chiarandini, C., Tsao, Y.S., Takatsuki, A., Adesnik, M., Sabatini, D.D., and Kreibich, G. (1992). *O*-Glycosylation of intact and truncated ribophorins in brefeldin A-treated cells: Newly synthesized intact ribophorins are only transiently accessible to the relocated glycosyltransferases. J. Cell Biol. **117,** 949–958.

Jako, C., Kumar, A., Wei, Y., Zou, J., Barton, D.L., Giblin, E.M., Covello, P.S., and Taylor, D.C. (2001). Seed-specific over-expression of an Arabidopsis cDNA encoding a diacylglycerol acyltransferase enhances seed oil content and seed weight. Plant Physiol. **126,** 861–874.

Jaworski, J., and Cahoon, E.B. (2003). Industrial oils from transgenic plants. Curr. Opin. Plant Biol. **6,** 178–184.

Katavic, V., Reed, D.W., Taylor, D.C., Giblin, E.M., Barton, D.L., Zou, J., Mackenzie, S.L., Covello, P.S., and Kunst, L. (1995). Alteration of seed fatty acid composition by an ethyl methanesulfonate-induced mutation in *Arabidopsis thaliana* affecting diacylglycerol acyltransferase activity. Plant Physiol. **108,** 399–409.

Kaup, M.T., Froese, C.D., and Thompson, J.E. (2002). A role for diacylglycerol acyltransferase during leaf senescence. Plant Physiol. **129,** 1616–1626.

Kennedy, E.P. (1961). Biosynthesis of complex lipids. Fed. Proc. **20,** 934–940.

Kim, H.U., Li, Y., and Huang, A.H.C. (2005). Ubiquitous and endoplasmic reticulum-located lysophosphatidyl acyltransferase, LPAT2, is essential for female but not male gametophyte development in Arabidopsis. Plant Cell **17,** 1073–1089.

Klopfenstein, D.R., Klumperman, J., Lustig, A., Kammerer, R.A., Oorschot, V., and Hauri, H.P. (2001). Subdomain-specific localization of CLIMP-63 (p63) in the endoplasmic reticulum is mediated by its luminal alpha-helical segment. J. Cell Biol. **153,** 1287–1300.

Krogh, A., Larsson, B., von Heijne, G., and Sonnhammer, E.L. (2001). Predicting transmembrane protein topology with a hidden Markov model: Application to complete genomes. J. Mol. Biol. **305,** 567–580.

Kusaka, T., Ishihara, S., Sakaida, M., Mifune, A., Nakano, Y., Tsuda, K., Ikeda, M., and Nakano, H. (1996). Composition analysis of normal plant triacylglycerols and hydroperoxidized rac-1-stearoyl-2-oleoyl-3-linoleoyl-sn-glycerols by liquid chromatography-atmospheric pressure chemical ionization mass spectrometry. J. Chromatogr. A. **730,** 1–7.

Lacey, D.J., and Hills, M.J. (1996). Heterogeneity of endoplasmic reticulum with respect to lipid synthesis in developing seeds of *Brassica napus* L. Planta **199,** 545–551.

Lardizabal, K.D., Mai, J.T., Wagner, N.W., Wyrick, A., Voelker, T., and Hawkins, D.J. (2001). DGAT2 is a new diacylglycerol acyltransferase gene family: purification, cloning, and expression in insect cells of two polypeptides from *Mortierella ramanniana* with diacylglycerol acyltransferase activity. J. Biol. Chem. **276,** 38862–38869.

Lee, M.S., Mullen, R.T., and Trelease, R.N. (1997). Oilseed isocitrate lyases lacking their essential type-1 peroxisomal targeting signal are piggybacked to glyoxysomes. Plant Cell **9,** 185–197.

Levine, T., and Rabouille, C. (2005). Endoplasmic reticulum: One continuous network compartmentalized by extrinsic cues. Curr. Opin. Cell Biol. **17,** 362–368.

Liu, P., Ying, Y., Zhao, Y., Mundy, D.I., Zhu, M., and Anderson, R.G.W. (2004). Chinese hamster ovary K2 cell lipid droplets appear to be metabolic organelles involved in membrane traffic. J. Biol. Chem. **279,** 3787–3792.

Lisenbee, C.S., Karnik, S.K., and Trelease, R.N. (2003). Overexpression and mislocalization of a tail-anchored GFP redefines the identity of peroxisomal ER. Traffic **4,** 491–501.

McCartney, A.W., Dyer, J.M., Dhanoa, P.K., Kim, P.K., Andrews, D.W., McNew, J.A., and Mullen, R.T. (2004). Membrane-bound fatty acid desaturases are inserted co-translationally into the ER and contain different ER retrieval motifs at their carboxy termini. Plant J. **37,** 156–173.

Milcamps, A., Tumaney, A.W., Paddock, T., Pan, D.A., Ohlrogge, J., and Pollard, M. (2005). Isolation of a gene encoding a 1,2-diacylglycerol-*sn*-acetyl-CoA acetyltransferase from developing seeds of *Euonymus alatus.* J. Biol. Chem. **280,** 5370–5377.

Murphy, D.J. (2001). The biogenesis and functions of lipid bodies in animals, plants and microorganisms. Prog. Lipid Res. **40,** 325–438.

Nehls, S., Snapp, E.L., Cole, N.B., Zaal, K.J., Kenworthy, A.K., Roberts, T.H., Ellenberg, J., Presley, J.F., Siggia, E., and Lippincott-Schwartz, J. (2000). Dynamics and retention of misfolded proteins in native ER membranes. Nat. Cell Biol. **2,** 288–295.

Newman, T., de Bruijn, F.J., Green, P., Keegstra, K., Kende, H., McIntosh, L., Ohlrogge, J., Raikhel, N., Somerville, S., Thomashow, M., Retzel, E., and Somerville, C. (1994). Genes galore: A summary of methods for accessing results from large-scale partial sequencing of anonymous Arabidopsis cDNA clones. Plant Physiol. **106,** 1241–1255.

Nilsson, T., Hoe, M.H., Slusarewicz, P., Rabouille, C., Watson, R., Hunte, F., Watzele, G., Berger, E.G., and Warren, G. (1994). Kin recognition between medial Golgi enzymes in HeLa cells. EMBO J. **13,** 562–574.

Nykiforuk, C.L., Furukawa-Stoffer, T.L., Huff, P.W., Sarna, M., Laroche, A., Moloney, M.M., and Weselake, R.J. (2002). Characterization of cDNAs encoding diacylglycerol acyltransferase from cultures of *Brassica napus* and sucrose-mediated induction of enzyme biosynthesis. Biochim. Biophys. Acta **1580,** 95–109.

Oelkers, P., Behari, A., Cromley, D., Billheimer, J.T., and Sturley, S.L. (1998). Characterization of two human genes encoding acyl coenzyme A:cholesterol acyltransferase-related enzymes. J. Biol. Chem. **273,** 26765–26771.

Oelkers, P., Cromley, D., Padamsee, M., Billheimer, J.T., and Sturley, S.L. (2002). The DGA1 gene determines a second triglyceride synthetic pathway in yeast. J. Biol. Chem. **277,** 8877–8881.

Ohlrogge, J., and Browse, J. (1995). Lipid biosynthesis. Plant Cell **7,** 957–970.

Page, R.D. (1996). TreeView: An application to display phylogenetic trees on personal computers. Comput. Appl. Biosci. **12,** 357–358.

Papp, S., Dziak, E., Michalak, M., and Opas, M. (2003). Is all of the endoplasmic reticulum created equal? The effects of the heterogeneous distribution of endoplasmic reticulum Ca^{2+}-handling proteins. J. Cell Biol. **160,** 475–479.

Rajasekharan, R., Marians, R.C., Shockey, J.M., and Kemp, J.D. (1993). Photoaffinity labeling of acyl-CoA oxidase with 12-azidooleoyl-CoA and 12-[(4-azidosalicyl)amino] dodecanoyl-CoA. Biochemistry **32,** 12386–12391.

Ramírez-Fajardo, A., Akoh, C.C., and Lai, O.M. (2003). Lipase-catalyzed incorporation of n-3 PUFA into palm oil. J. Am. Oil Chem. Soc. **80,** 1197–1200.

Routaboul, J.M., Benning, C., Bechtold, N., Caboche, M., and Lepiniec, L. (1999). The TAG1 locus of Arabidopsis encodes for a diacylglycerol acyltransferase. Plant Physiol. Biochem. **37,** 831–840.

Sabnis, R.W., Deligeorgiev, T.G., Jachak, M.N., and Dalvi, T.S. (1997). $DiOC_6(3)$: A useful dye for staining the endoplasmic reticulum. Biotech. Histochem. **72,** 253–258.

Sambrook, J., Fritsch, E.F., and Maniatis, T. (1989). Molecular Cloning: A Laboratory Manual, 2nd ed. (Cold Spring Harbor, NY: Cold Spring Harbor Laboratory Press).

Scott, A., Wyatt, S., Tsou, P.-L., Robertson, D., and N.S. Allen. (1999). Model system for plant cell biology: GFP imaging in living onion epidermal cells. Biotechniques **26,** 1125–1132.

Settlage, S.B., Wilson, R.F., and Kwanyuen, P. (1995). Localization of diacylglycerol acyltransferase to oil body associated endoplasmic reticulum. Plant Physiol. Biochem. **33,** 399–407.

Shan, S.O., and Walter, P. (2005). Co-translational protein targeting by the signal recognition particle. FEBS Lett. **579,** 921–926.

Shanklin, J., and Cahoon, E.B. (1998). Desaturation and related modifications of fatty acids. Annu. Rev. Plant Physiol. Plant Mol. Biol. **49,** 611–641.

Shockey, J.M., Dhanoa, P.K., Dupuy, T., Chapital, D.C., Mullen, R.T., and Dyer, J.M. (2005). Cloning, functional analysis, and subcellular localization of two isoforms of NADH:cytochrome b_5 reductase from developing seeds of tung (*Vernicia fordii*). Plant Sci. **169,** 375–385.

Singh, S.P., Zhou, X.-R., Liu, Q., Stymne, S., and Green, A.G. (2005). Metabolic engineering of new fatty acids in plants. Curr. Opin. Plant Biol. **8,** 197–203.

Smirnova, E., Goldberg, E.B., Makarova, K.S., Lin, L., Brown, W.J., and Jackson, C.L. (2006). ATGL has a key role in lipid droplet/adiposome degradation in mammalian cells. EMBO Rep. **7,** 106–113.

Snapp, E.L., Hegde, R.S., Francolini, M., Lombardo, F., Colombo, S., Pedrazzini, E., Borgese, N., and Lippincott-Schwartz, J. (2003). Formation of stacked ER cisternae by low affinity protein interactions. J. Cell Biol. **163,** 257–269.

Sonntag, N.O.V. (1979). Composition and characteristics of individual fats and oils. In Bailey's Industrial Oil and Fat Products, Vol. 1, D. Swern, ed. (New York: John Wiley & Sons), pp. 289–477.

Staehelin, L.A. (1997). The plant ER: A dynamic organelle composed of a large number of discrete functional domains. Plant J. **11,** 1151–1165.

Ståhl, U., Carlsson, A.S., Lenman, M., Dahlqvist, A., Huang, B., Banas, W., Banas, A., and Stymne, S. (2004). Cloning and functional characterization of a phospholipid:diacylglycerol acyltransferase from Arabidopsis. Plant Physiol. **135,** 1324–1335.

Thaminy, S., Miller, J., and Stagljar, I. (2004). The split-ubiquitin membrane-based yeast two-hybrid system. Methods Mol. Biol. **261,** 297–312.

Thelen, J.J., and Ohlrogge, J.B. (2002). Metabolic engineering of fatty acid biosynthesis in plants. Metab. Eng. **4,** 12–21.

Thompson, J.D., Gibson, T.J., Plewniak, F., Jeanmougin, F., and Higgins, D.G. (1997). The ClustalX windows interface: Flexible strategies for multiple sequence alignment aided by quality analysis tools. Nucleic Acids Res. **24,** 4876–4882.

Uemura, T., Ueda, T., Ohniwa, R., Nakano, A., Takeyasu, K., and Sato, M.H. (2004). Systematic analysis of SNARE molecules in Arabidopsis: Dissection of the post-Golgi network in plant cells. Cell Struct. Funct. **29,** 49–65.

van de Loo, F.J., Broun, P., Turner, S., and Somerville, C. (1995). An oleate 12-hydroxylase from *Ricinus communis* L. is a fatty acyl desaturase homolog. Proc. Natl. Acad. Sci. USA **92,** 6743–6747.

Vogel, G., and Browse, J. (1996). Cholinephosphotransferase and diacylglycerol acyltransferase (substrate specificities at a key branch point in seed lipid metabolism). Plant Physiol. **110,** 923–931.

Wan, C.Y., and Wilkins, T.A. (1994). A modified hot borate method significantly enhances the yield of high-quality RNA from cotton (*Gossypium hirsutum* L.). Anal. Biochem. **223,** 7–12.

Zacharias, D.A., Violin, J.D., Newton, A.C., and Tsien, R.Y. (2002). Partitioning of lipid-modified monomeric GFPs into membrane microdomains of live cells. Science **296,** 913–916.

Zheng, Z., Xia, Q., Dauk, M., Shen, W., Selvaraj, G., and Zou, J. (2003). AtGPAT1, a member of the membrane-bound glycerol-3-phosphate acyltransferase gene family, is essential for tapetum differentiation and male fertility. Plant Cell **15,** 1872–1887.

Zou, J., Wei, Y., Jako, C., Kumar, A., Selvaraj, G., and Taylor, D.C. (1999). The *Arabidopsis thaliana* TAG1 mutant has a mutation in a diacylglycerol acyltransferase gene. Plant J. **19,** 645–653.